Optical and Quantum Electronics **23** *(1991) 727–754*

Theoretical analysis of pulse development in a colliding pulse mode-locked dye laser

A. PENZKOFER, W. BÄUMLER
Naturwissenschaftliche Fakultät II – Physik, Universität Regensburg, W-8400 Regensburg, FRG

Received 7 December 1990; revised 11 March; accepted 21 March 1991

The pulse development in colliding pulse mode-locked dye lasers is analysed theoretically. The chosen parameters belong to a c.w. argon laser pumped linear resonator arrangement with rhodamine 6G in ethylene glycol as gain medium and DODCI (3,3'-diethyloxadicarbocyanine iodide) in ethylene glycol as saturable absorber. The pulse shortening and pulse broadening effects in the laser oscillator are investigated. The steady-state pulse duration is determined by equal pulse broadening and pulse shortening within a single resonator round-trip. The detuning of the absorber jet out of the middle position of the resonator is considered. Multiple transits through the resonator are simulated to study the influence of various resonator and dye parameters on the pulse development and the background signal suppression. Fast relaxations within the S_1 and S_0-state of DODCI are necessary for sufficient background suppression to obtain femtosecond pulse trains.

1. Introduction

Colliding pulse mode-locked (CPM) dye lasers are used widely to generate femtosecond light pulses [1–4]. The colliding pulse mode-locking was achieved in ring lasers [1] and in linear resonators including either an anti-resonant ring [4, 5], a contacted absorber cell [6] or an absorber cell in the middle of the cavity [3, 7]. Various gain dye–absorber dye combinations were applied to cover the spectral region from 497 nm [8] to 974 nm [9] (for surveys see [3, 4]). The most widely applied gain–absorber combination is rhodamine 6G in ethylene glycol and DODCI (3,3'-diethyloxadicarbocyanine iodide) in ethylene glycol. For this gain–absorber pair pulse durations down to 20 fs have been generated around 620 nm [10, 11] in a prism balanced colliding pulse mode-locked laser arrangement [12].

The passive mode-locking in c.w. pumped dye lasers was analysed theoretically in [13–33]. The action of slow saturable absorber bleaching and gain dye depletion was studied in [13–16]. An analytical solution was given by including dispersive bandwidth limiting effects [17]. The colliding pulse intensity enhancement [18, 19] and transient grating effects were included in [20, 21]. The chirp production in CPM dye lasers was discussed and off-resonance interactions were considered in [22]. The effects of self-phase modulation, group velocity dispersion, and chirp compensation were studied in [23–31]. The soliton pulse formation [32] in CPM lasers was discussed in [33].

0306-8919/91 $03.00 + .12

This paper gives a detailed simulation of the pulse development in a c.w. pumped linear colliding pulse mode-locked rhodamine 6G DODCI dye laser. A realistic absorber dye and a realistic gain dye model are solved numerically by a rate equation approach. For the saturable absorber the influences of the fast Franck-Condon relaxation time in the S_1-state and of the fast spectral cross-relaxation time in the S_0-ground-state are analysed. The obtainable steady-state pulse durations due to the pulse shortening by absorber bleaching and the pulse broadening by dispersive effects are estimated by considering a single resonator round-trip. The pulse shortening by compensation of group velocity dispersion and by self-phase modulation combined with intracavity pulse compression is discussed shortly. The effects of detuning the absorber jet out of the colliding pulse mode-locking position of the linear resonator are studied.

In the simulation of multiple round-trips the combined action of pulse shortening and background suppression of the absorber and gain medium are analysed. The optimum intensities in the absorber and gain medium are determined. The necessity of fast relaxation within the S_1 and S_0 band of the saturable absorber DODCI for background suppression and femtosecond pulse generation is shown.

The repetitive pulse shortening action of the slow absorber DODCI in a CPM dye laser has been studied recently by numerical simulations where the gain medium was assumed to compensate only the absorption losses (no pulse shaping action of the gain medium) [34].

2. Absorber and gain model

The linear CPM dye laser is sketched in Fig. 1a. The saturable absorber is in the middle of the resonator and the gain medium is located one quarter away from the output mirror. In

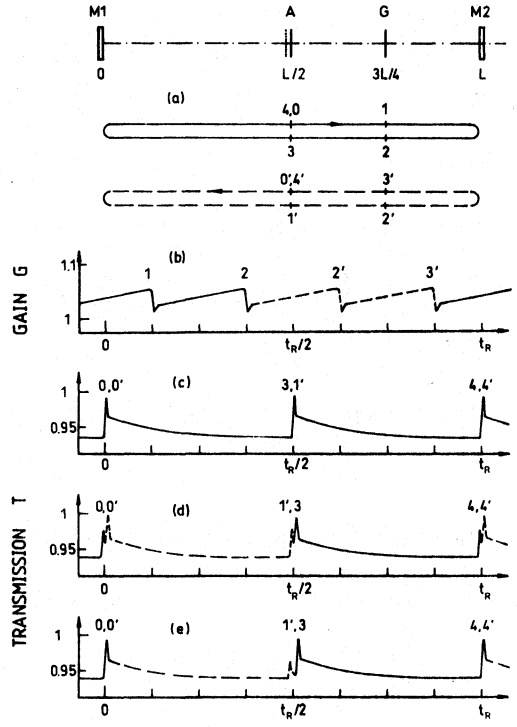

Figure 1 Linear CPM dye laser. (a) Schematic arrangement. M1, 100% mirror. M2, output mirror with reflectivity R_{out}. G, gain jet. A, absorber jet; (——) bar indicates ideal position at $L/2$, and (- - -) bar indicates detuned position. The circulation of the clockwise (——) and the counter-clockwise (- - -) rotating pulses are illustrated. (b) Illustration of time dependent amplification in gain jet. (c–e) Illustration of time dependent transmission through absorber jet in the case of ideal position at centre of cavity (c) and in the case of detuned position (d, e). (d) shows symmetric passage of the counter-propagating pulses. (e) displays an asymmetric passage where the pulses collide once per round-trip in the absorber jet.

the resonator two pulses propagate in opposite direction. They pass simultaneously through the absorber jet. The absorber is bleached by the concerted action of the colliding pulses in the absorber jet (Fig. 1c). After pulse passage the absorption recovers before the next transit. The circulating pulses pass through the absorber in time intervals of half the resonator round trip time t_R. In time intervals of one quarter of the round trip time the pulses are amplified in the gain jet (Fig. 1b). Through the output mirror part of the circulating pulse energy is transmitted so that a continuous pulse train is generated. The time interval between adjacent output pulses is half the resonator round-trip time.

2.1. Rate equations for saturable absorber

The saturable absorption of DODCI has been studied in detail recently, where the photoisomerization dynamics was included [34]. Here the coupling dynamics between the *N* and *P*-isomers is neglected. Only steady-state mole fractions for the *N*- and *P*-isomers are used. The long-wavelength excitation (λ_L = 620 nm) and the short wavelength excitation (λ_L = 580 nm) are considered. The equation system for the long-wavelength absorber bleaching is given below (Equations 1 to 7) while the equation system for the short wavelength excitation is written in Appendix A.

The long-wavelength excitation scheme is illustrated in Fig. 2b. The relevant equation system for the absorber bleaching is

$$\frac{\partial N_{1N}}{\partial t'} = -\frac{\sigma_N}{h\nu_L}(N_{1N^*} - N_{2N})\kappa I_{L,A} + \frac{N_{2N}}{\tau_N} \tag{1}$$

$$\frac{\partial N_{1N^*}}{\partial t'} = -\frac{\sigma_N}{h\nu_L}(N_{1N^*} - N_{2N})\kappa I_{L,A} - \frac{N_{1N^*} - \rho_N N_{1N}}{T_3} \tag{2}$$

$$\frac{\partial N_{2N}}{\partial t'} = \frac{\sigma_N}{h\nu_L}(N_{1N^*} - N_{2N})\,\kappa I_{L,A} - \frac{N_{2N}}{\tau_N} \tag{3}$$

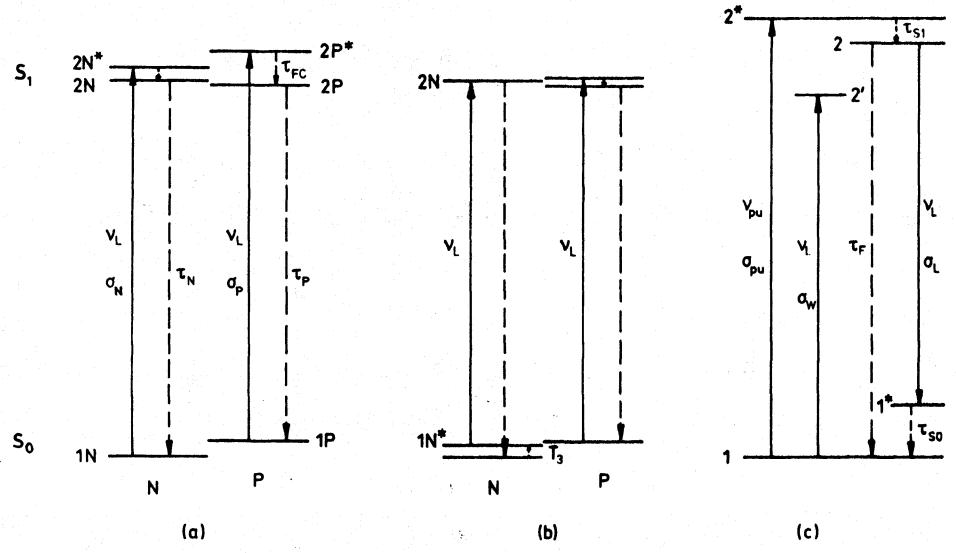

Figure 2 Level diagrams for (a) short-wavelength excitation of absorber DODCI, (b) long-wavelength excitation of absorber DODCI, and (c) gain medium rhodamine 6G. *N*, normal form of DODCI. *P*, photoisomer of DODCI.

$$\frac{\partial N_{1P}}{\partial t'} = -\frac{\sigma_P}{h\nu_L}(N_{1P} - N_{2P^*})\kappa I_{L,A} + \frac{N_{2P} + N_{2P^*}}{\tau_P} \tag{4}$$

$$\frac{\partial N_{2P^*}}{\partial t'} = \frac{\sigma_P}{h\nu_L}(N_{1P} - N_{2P^*})\kappa I_{L,A} - \frac{N_{2P^*}}{\tau_{FC}} - \frac{N_{2P^*}}{\tau_P} \tag{5}$$

$$\frac{\partial N_{2P}}{\partial t'} = \frac{N_{2P^*}}{\tau_{FC}} - \frac{N_{2P}}{\tau_P} \tag{6}$$

$$\frac{\partial I_{L,A}}{\partial z'} = -I_{L,A}[\sigma_N(N_{1N^*} - N_{2N}) + \sigma_P(N_{1P} - N_{2P^*})] \tag{7}$$

The transformations $t' = t - n_A z/c_0$ and $z' = z$ are used, where t is the time, n_A is the refractive index of the absorber solution, z is the distance along the propagation direction, and c_0 is the velocity of light in vacuum. Inter-isomer transitions between the N- and P-isomers are neglected. Absorption anisotropy [35] and excited-state absorption [36] are not included. σ_N and σ_P are the N-isomer and P-isomer absorption cross-sections at the laser wavelength. τ_N and τ_P are the absorption recovery times of the N- and P-isomers, respectively. τ_{FC} is the relaxation time out of the excited Franck-Condon state to the relaxed S_1 levels. T_3 is the spectral cross-relaxation time in the ground state. It gives the repopulation time (thermalization time) of the level $1N^*$.

The factor κ in the equations takes care of the fact that two pulses, each of intensity I_L, are colliding in the absorber cell. In our calculations we set $\kappa = 2$ neglecting the coherence effects in the pulse overlap region which lead to $\kappa = 3$ [4, 18, 19].

The initial conditions of the level populations are $N_{1N}(t' = -\infty, z) = (1 - x_P)N_A$, $N_{1N^*}(t' = -\infty, z) = (1 - x_P)\rho_N N_A$, $N_{2N}(t' = -\infty, z) = 0$, $N_{1P}(t' = -\infty, z) = x_P N_A$, $N_{2P}(t' = -\infty, z) = N_{2P^*}(t' = -\infty, z) = 0$. x_P gives the mole fraction of P isomers. It is set to an accumulated steady-state value [37]. ρ_N is the fraction of N-isomer molecules which take part in the long-wavelength excitation process [38, 39]. This fraction is given by

$$\rho_N = \exp\left[-\frac{h(\nu_{N12} - \nu_L)}{k_B\theta}\right] \tag{8}$$

where ν_{N12} is the electronic S_0–S_1 transition frequency of the N-isomers, k_B is the Boltzmann constant, h is the Planck's constant, and θ is the temperature. The level population N_{1N} includes N_{1N^*}. The dye number density N_A determines the small-signal absorber transmission T_0 according to

$$T_0 = \exp\{-[(1 - x_P)\rho_N\sigma_N + x_P\sigma_P]N_A l_A\} \tag{9}$$

[34] where l_A is the absorber jet thickness.

In the time period $t_R/2$ between the pulse transits through the absorber the level populations recover to the initial conditions with the decay constants τ_N and τ_P.

2.2. Rate equations for gain medium

The active medium is described by the level scheme of Fig. 2c. In the calculations a c.w. argon ion laser pumped rhodamine 6G dye jet is simulated. The pump light of intensity I_{pu} and frequency ν_{pu} is continuous while the generated laser light of intensity $I_{L,G}$ and frequency ν_L is repetitive with a recurrence interval of $t_R/4$ and a pulse duration Δt_L in the subpicosecond region. The population of the upper pump laser level 2* remains small all the time

since the Franck-Condon relaxation time τ_{S_1} is short compared to the pulse recurrence interval $t_R/4$. The amplifier equation system reads

$$\frac{\partial N_1}{\partial t'} = -\frac{\sigma_{pu}}{h\nu_{pu}} I_{pu} N_1 + \frac{N_2}{\tau_F} \frac{N_1}{N_1 + N_{1\bullet}} + \frac{N_{1\bullet}}{\tau_{S0}} \tag{10}$$

$$\frac{\partial N_2}{\partial t'} = \frac{\sigma_{pu}}{h\nu_{pu}} I_{pu} N_1 - \frac{N_2}{\tau_F} - \frac{\sigma_L}{h\nu_L} I_{L,G}(N_2 - N_{1\bullet}) \tag{11}$$

$$\frac{\partial N_{1\bullet}}{\partial t'} = \frac{\sigma_L}{h\nu_L} I_{L,G}(N_2 - N_{1\bullet}) - \frac{N_1^*}{\tau_{S0}} + \frac{N_2}{\tau_F} \frac{N_{1\bullet}}{N_1 + N_{1\bullet}} \tag{12}$$

$$\frac{\partial I_{pu}}{\partial z'} = -\sigma_{pu} I_{pu} N_1 \tag{13}$$

$$\frac{\partial I_{L,G}}{\partial z'} = \sigma_L I_{L,G}(N_2 - N_{1\bullet}) - \sigma_W I_{L,G} N_1 \tag{14}$$

The initial conditions of the level populations are $N_1(z,\ t' = -\infty) = N_G$, $N_{1\bullet}(z,\ t' = -\infty) = N_2(x, t' = -\infty) = 0$. The term $\sigma_W I_{L,G} N_1$ in Equation 14 describes the laser light reabsorption in the long-wavelength absorption wing of rhodamine 6G in ethylene glycol (see Fig. 8).

3. Steady-state simulations of one round-trip

In the following the various pulse shortening and pulse broadening effects are studied for a single pulse round-trip in the resonator. Pulse shortening occurs mainly by the saturable absorber bleaching and pulse broadening is mainly due to group velocity dispersion in the dye jets (temporal pulse chirp). The equating of pulse shortening and pulse broadening in the steady state gives an estimate of the obtainable pulse duration in a CPM laser. The frequency chirp of the pulses by self-phase modulation is described. The pulse shortening by compensation of group velocity dispersion [12, 40] and by compression of self-phase modulated pulses [41, 42] in prism pairs [10–12, 43–47], mirrors [48, 49], and interferometers [50, 51] is discussed shortly. The influence of the absorber jet shifting out of the centre position of the resonator is considered.

3.1. Pulse shortening by saturable absorption in loss jet

The small-signal single-pass transmission through the saturable absorber is set to $T_0 = 0.95$ for the thermal N-isomer and P-isomer distribution ($x_p = x_{p,th}$ in Equation 9) in the calculations. Under steady-state lasing conditions the P-isomer accumulation is taken into account by an approximate x_P-value (see Table 1 and [34, 37]). The input pulse shape is assumed to be Gaussian. The behaviour of DODCI in ethylene glycol at 620 and 580 nm is simulated. The used parameters are collected in Table 1. At 620 nm the absorption cross-section σ_N of the interacting N-isomers is given by σ_{em}^N [38, 39] (see Fig. 13). The time-integrated transmission versus input peak intensity is depicted in Fig. 3 and the pulse shortening ratio $\beta_A = \Delta t_{L,out}/\Delta t_{L,in}$ versus input peak intensity $I_{0L,A}$ is shown in Fig. 4. Curves for various input pulse durations are calculated. The optimum input peak intensity $I_{0L,opt}^A$ for maximum pulse shortening is plotted versus input pulse duration in Fig. 5. $I_{0L,opt}^A$ is inversely proportional to the pulse duration (this situation applies for slow saturable absorbers $\Delta t_L \ll \tau_A$ [34, 52] where τ_A is the absorption recovery time). The optimum

TABLE 1 Parameters of CPM resonator, absorber medium and gain medium

Parameter	Wavelength		References
	580 nm	620 nm	
Resonator:			
R_{out}	0.97	0.97	-
t_R (ns)	16.6	16.6	-
Gain medium: rhodamine 6G in ethylene glycol (Fig. 2c).			
λ_{pu} (nm)		514	
l_G (mm)	0.25	0.25	-
σ_{pu} (cm^2)	2×10^{-16}	2×10^{-16}	Fig. 8
τ_F (ns)	4.1	4.1	a
τ_{SO} (ps)	4	4	[110]
G_0	1.072	1.068	-
σ_L (cm^2)	2.2×10^{-16}	9×10^{-17}	Fig. 8
$\varepsilon^G_{sat,s}$ ($J\,cm^{-2}$)	1.55×10^{-3}	3.56×10^{-3}	Eq. 18
N_G (cm^{-3})	1.2×10^{18}	1.2×10^{18}	-
$N_{2,0}$ (cm^{-3})	1.5×10^{16}	1.8×10^{16}	Eq. 34
I_{pu} ($W\,cm^{-2}$)	4.8×10^4	5.4×10^4	Eq. 35
Loss medium: DODCI in ethylene glycol			
Level system	Fig. 2a	Fig. 2b	-
$x_{p,th}$	0.029	0.029	[58]
x_p	0.25	0.10	[34,37]
ρ_N	1	0.06	Eq. 8
σ_N (cm^2)	7.25×10^{-16}	7×10^{-16}	Fig. 13
σ_P (cm^2)	1.9×10^{-16}	5.2×10^{-16}	Fig. 13
$\varepsilon^A_{sat,s}$ ($J\,cm^{-2}$)	5.11×10^{-4}	5.12×10^{-4}	Eq. 15
τ_N (ns)	1.3	1.3	[37]
τ_P (ns)	1.4	1.4	[37]
τ_{FC} (ps)	0.95	0.95	[109]
T_3 (ps)	1	1	assumed
$\tilde{\nu}_{N12}$ (cm^{-1})	16710	16710	[37]
T_0	0.95	0.95	-
l_A (μm)	35	35	-

a: own measurement

intensities at $\lambda_L = 580$ nm and at $\lambda_L = 620$ nm are practically the same. The optimum pulse energy density $\varepsilon^A_{opt} = I^A_{0L,opt} \int_{-\infty}^{\infty} \exp(-t/t_0)^2 dt = \pi^{1/2} t_0 I^A_{0L,opt} = 0.5[\pi/\ln 2]^{1/2} \Delta t_L I^A_{0L,opt}$ versus pulse duration Δt_L is included in Fig. 5. It is approximately constant for $\Delta t_L \leqslant 1$ ps.

The optimum pulse energy density ε^A_{opt} should be compared with the saturation energy density $\varepsilon^A_{sat,s} = \Delta t_L I^A_{sat,s}$ of the slow saturable absorber. $\varepsilon^A_{sat,s}$ is given by [34]

$$\varepsilon^A_{sat,s} = \frac{h\nu_L}{\rho_N(1 - x_p) + x_p} \left[\frac{\rho_N(1 - x_p)}{\sigma_N} + \frac{x_p}{\sigma_p} \right] \tag{15}$$

$\varepsilon^A_{sat,s}$ and $I^A_{sat,s}$ are included in Fig. 5. Optimum pulse shortening occurs for $I_{0L,A}$ slightly above $I^A_{sat,s}$. For the curves of Figs 3 and 4 belonging to $\Delta t_{L,in} = 1$ ps the $I^A_{sat,s}$ values are indicated by bars.

The temporal pulse shortening per round-trip in the resonator is the square of the single-pass shortening factor. The optimum pulse shortening per round-trip versus input

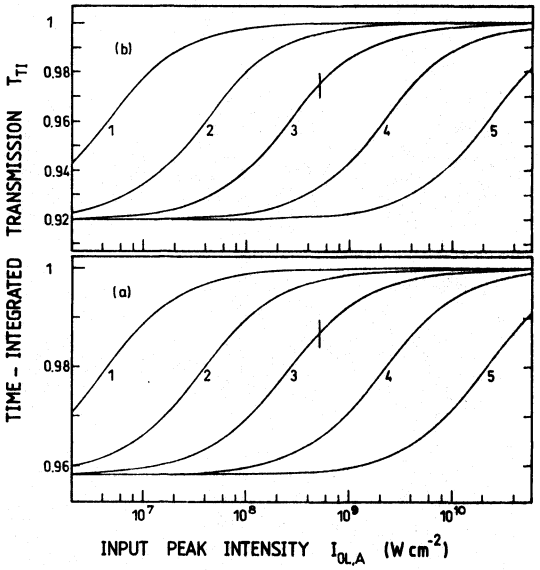

Figure 3 Bleaching of saturable absorber DODCI in etyhlene glycol in single passage under repetitive circulation condition. (a) λ_L = 580 nm. (b) λ_L = 620 nm. The curves belong to input pulse durations of $\Delta t_{L,in}$ = 100 ps (1), 10 ps (2), 1 ps (3), 100 fs (4), and 10 fs (5). The bar on curve 3 indicates the saturation intensity $I^A_{sat,a}$ of the slow saturable absorber (see Equation 15). Applied absorber parameters are collected in Table 1.

pulse duration is displayed in Fig. 6. The temporal shortening δt_A is proportional to the input pulse duration $\Delta t_{L,in}$.

The absorption recovery of the mode-locking dye is displayed in Fig. 7. The transmission of a weak probe T_{pr} versus time is shown for three different input pulse durations. For $\Delta t_{L,in} < T_3$ (Fig. 7b) or $\Delta t_{L,in} < \tau_{FC}$ (Fig. 7a) the transmission decreases partially with a slope proportional to T_3 or τ_{FC}. This partial absorption recovery is important for the

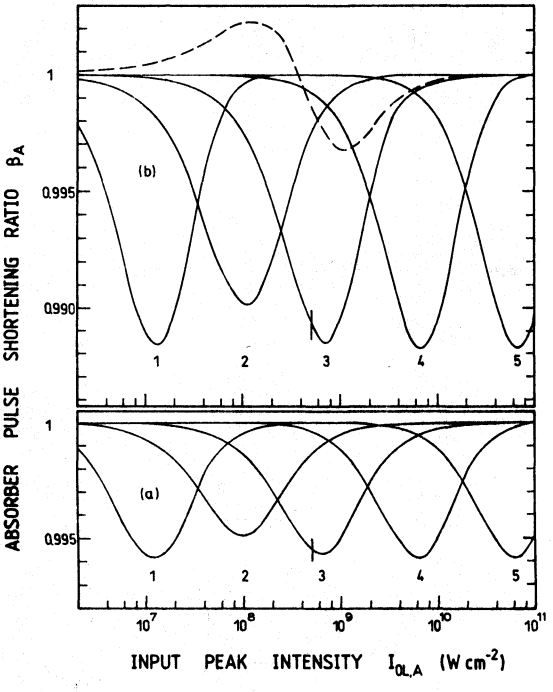

Figure 4 Pulse shortening ratio in a single passage through absorber jet. (a) λ_L = 580 nm. (b) λ_L = 620 nm. The (– – –) curves belong to same parameters as in Fig. 3. The (– · –) curve is calculated for an asymmetric Gaussian pulse of $\Delta t_L = \Delta t_{L_1} + \Delta t_{L_2}$ = 1 ps duration with $\Delta t_{L_1}/\Delta t_{L_2}$ = 0.5.

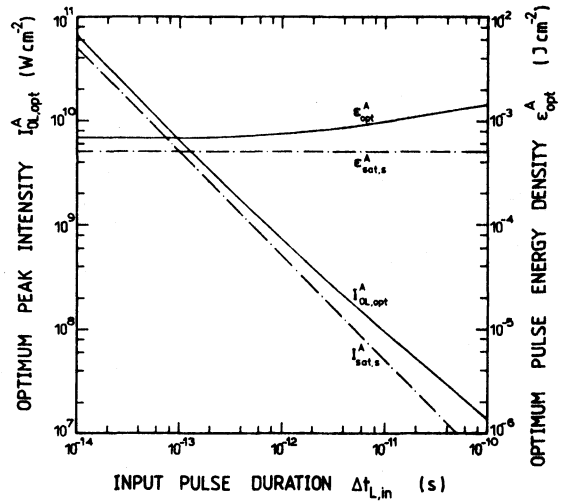

Figure 5 Optimum peak intensity $I^A_{0L,opt}$ and optimum energy density ε^A_{opt} for maximum pulse shortening in absorber jet (– – –). $I^A_{0L,opt}$ is derived from Fig. 4. The slow saturation intensity $I^A_{sat,s}$ and the slow saturation energy density $\varepsilon^A_{sat,s}$ (Equation 15) are included (– · – · –). Curves apply to λ_L = 620 nm. The curves for 580 nm are practically identical.

background signal suppression [34] (see below). The final recovery is determined by the relaxation times τ_N and τ_P.

3.2. Pulse broadening by amplification depletion in gain jet

The pulse propagation through the gain medium is described by the Equations 10 to 14. The time period between the repetitive passage through the gain medium is $t_R/4$. In the following single passage calculations the pump laser intensity I_{pu} is adjusted in such a way that the small-signal round-trip amplification compensates the small-signal round-trip losses. The

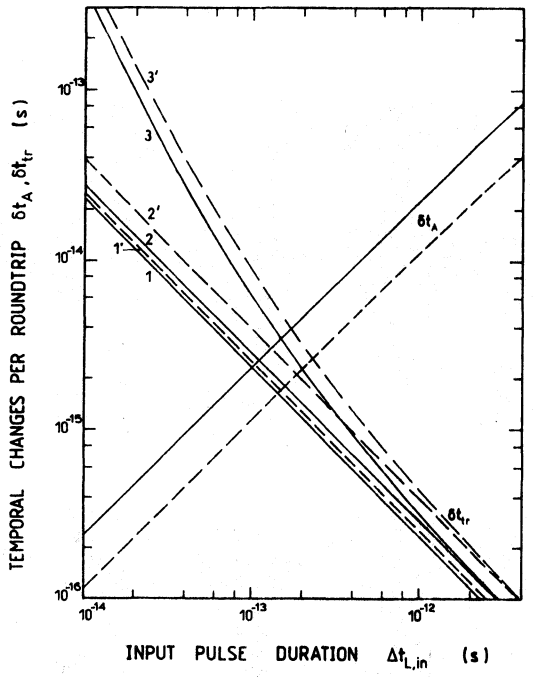

Figure 6 Temporal changes per round-trip. The δt_A curves give the optimum pulse duration shortening per round-trip. Data belong to Fig. 4 and Table 1. The δt_{tr} curves show transit time broadenings due to (1, 1') group velocity dispersion of the solvent, (2, 2') group velocity dispersion of the absorber and gain dye solution, and (3, 3') due to group velocity dispersion and frequency chirp in absorber and gain jet. Data of Fig. 12 and Table 1 are applied. The (——) curves belong to λ_L = 620 nm, the (– – –) curves belong to λ_L = 580 nm.

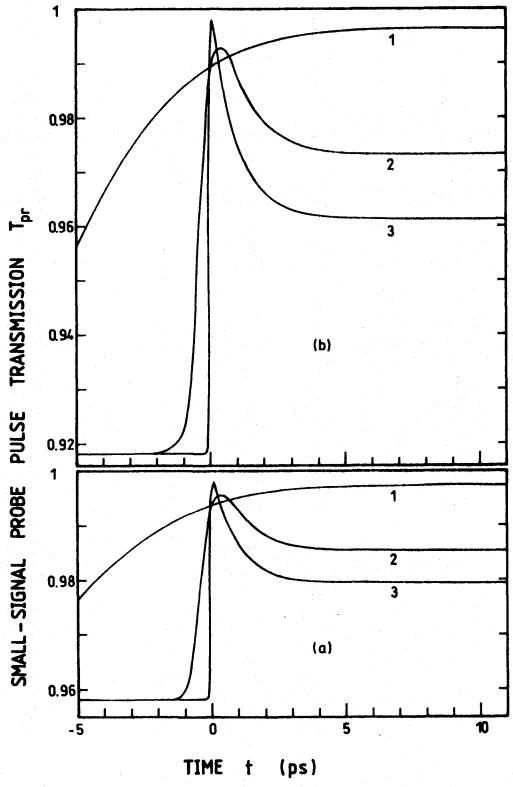

Figure 7 Absorption recovery in absorber jet. The small-signal transmissions belong to (1) $\Delta t_{L,in}$ = 10 ps, (2) $\Delta t_{L,in}$ = 1 ps and (3) $\Delta t_{L,in}$ = 0.1 ps. The pump laser peak intensity is set to $I^{\wedge}_{0L,opt}(\Delta t_{in})$ (see Fig. 5). The absorber parameters of Fig. 3 and Table 1 are applied. (a) Wavelength λ_L = 580 nm. (b) λ_L = 620 nm.

small-signal gain per passage is $G_0 = \exp[(N_{2,0}\sigma_L - N_{1,0}\sigma_W)l_G]$, where $N_{2,0}$ is the initial upper laser level population and $N_{1,0}$ is the initial ground-state population. σ_W gives the ground-state absorption cross-section at the laser frequency. The total small-signal gain per round-trip is G_0^2 and the total small-signal reduction per round-trip is $T_0^2 R_{out}$, where T_0 is the small-signal single-pass transmission of the absorber and R_{out} is the output mirror reflectivity. The loss compensation leads to $G_0 = (T_0 R_{out}^{1/2})^{-1}$.

Calculations are carried out for laser wavelengths of λ_L = 620 nm and λ_L = 580 nm. The applied dye parameters are listed in Table 1. They belong to rhodamine 6G in ethylene glycol. The apparent absorption and emission cross-section spectra of rhodamine 6G in ethylene glycol are shown in Fig. 8.

In Fig. 9 the time integrated gain

$$G_{TI} = \frac{\int_{-\infty}^{\infty} I_{L,G}(t', l_G)\,dt'}{\int_{-\infty}^{\infty} I_{L,G}(t', 0)\,dt'} \tag{16}$$

versus input laser peak intensity $I_{0L,G}$ is shown for various input laser pulse duractions. The gain G_{TI} reduces with increasing input intensity. Since the fluorescence lifetime of the upper laser level is long compared to the input pulse duration one may speak of a slow gain medium and the gain reduction is characterized by a slow gain saturation intensity

$$I^{G}_{sat,s} = \frac{h\nu_L}{\sigma_L \Delta t_L} \tag{17}$$

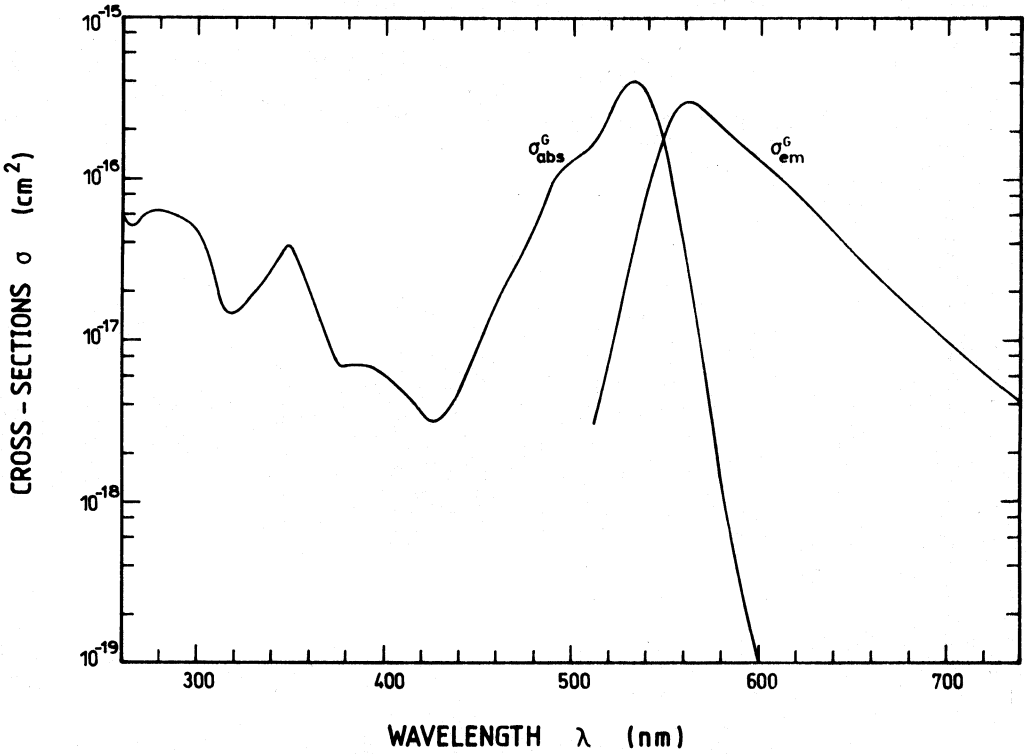

Figure 8 Absorption and emission cross-section spectrum of rhodamine 6G in ethylene glycol.

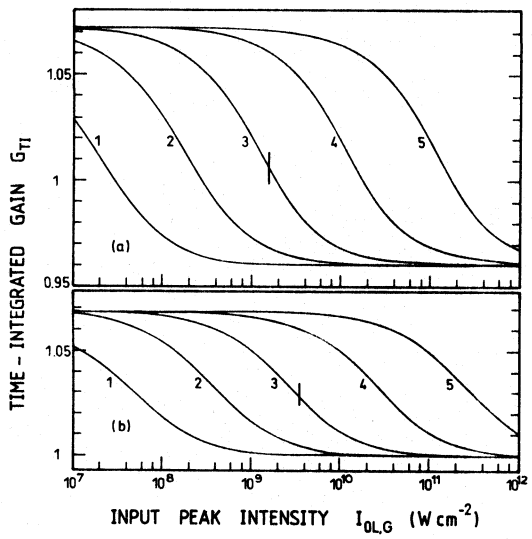

Figure 9 Gain depletion of rhodamine 6G in ethylene glycol in a single passage through gain jet. (a) λ_L = 580 nm. (b) λ_L = 620 nm. The curves belong to symmetric Gaussian input pulses of durations $\Delta t_{L,in}$ = 100 ps (1), 10 ps (2), 1 ps (3), 100 fs (4), and 10 fs (5). Practically the same curves are obtained for asymmetric Gaussian pulses. The bars on curves 3 indicates the saturation intensities of the slow gain medium (see Equation 17). Applied dye parameters are listed in Table 1.

or a slow gain saturation energy density

$$\varepsilon^{G}_{sat,s} = \frac{h\nu_L}{\sigma_L} \tag{18}$$

where σ_L is the stimulated emission cross-section at the laser frequency. For the curves belonging to $\Delta t_{L,in} = 1$ ps the $I^{G}_{sat,s}$ values are indicated by bars in Fig. 9.

At $\lambda_L = 580$ nm there is still some ground-state absorption left. Therefore, in the case of complete gain bleaching at high input intensities the residual absorption dominates leading to signal reduction in the gain medium ($G_{TI} < 1$).

The change of pulse duration versus input laser peak intensity is displayed in Fig. 10 for various input pulse durations. For symmetric Gaussian pulses, the nonlinear gain depletion leads to a broadening of the pulse duration (FWHM). The rising part of the pulses is predominantly amplified compared to the pulse maximum leading to a pulse broadening. The pulse broadening is largest around $I_{0L,G} \approx 2.5 \times I^{G}_{sat,s}$.

The pulse shaping behaviour of an asymmetric Gaussian pulse in the gain medium is illustrated by the dashed curves in Fig. 10 belonging to $\Delta t_{L,in} = 1$ ps. In the displayed case the half-width of the rising part Δt_{L-} is half the half-width of the trailing part Δt_{L+} ($\Delta t_{L-} = 0.5\Delta t_{L+}$, $\Delta t_{L-} + \Delta t_{L+} = \Delta t_L$). In this case there occurs a pulse shortening up to $I_{0L} \approx 1.7 I^{G}_{sat,s}$ and a pulse broadening at higher pulse peak intensities. The pulse shaping of this asymmetric Gaussian pulse in the absorber is illustrated by the dashed curve in Fig. 4b. There the pulse reshaping by saturable absorption leads to a pulse broadening for $I_{0L} \leqslant 0.75 I^{A}_{sat,s}$ and then to a pulse shortening. The combined pulse shaping of the absorber and the gain medium in repetitive transits is studied below in Section 4.

For the rhodamine 6G-DODCI dye combination the saturation intensity of the gain medium is higher than the saturation intensity of the absorber medium (see Table 1). In real CPM lasers the beam diameter in the gain jet is made larger than in the absorber jet (mirror

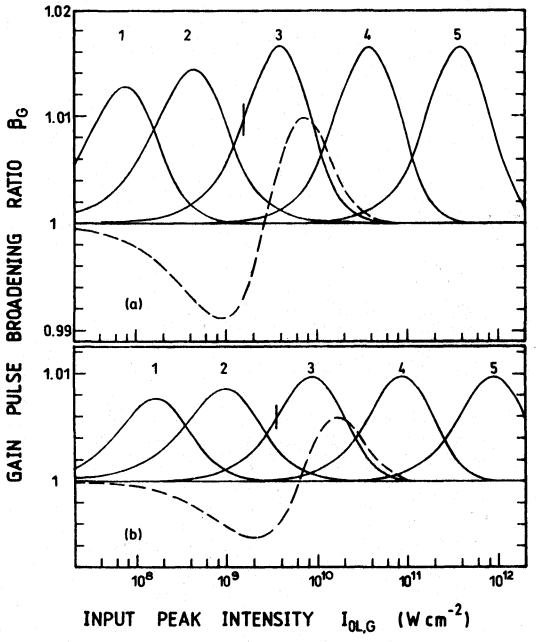

Figure 10 Pulse broadening ratio in a single passage through gain jet. (a) $\lambda_L = 580$ nm. (b) $\lambda_L = 620$ nm. The (——) curves belong to the same parameters as in Fig. 9. The (– – –) curves are calculated for an asymmetric Gaussian pulse of 1 ps duration with $\Delta t_{L-}/\Delta t_{L+} = 0.5$.

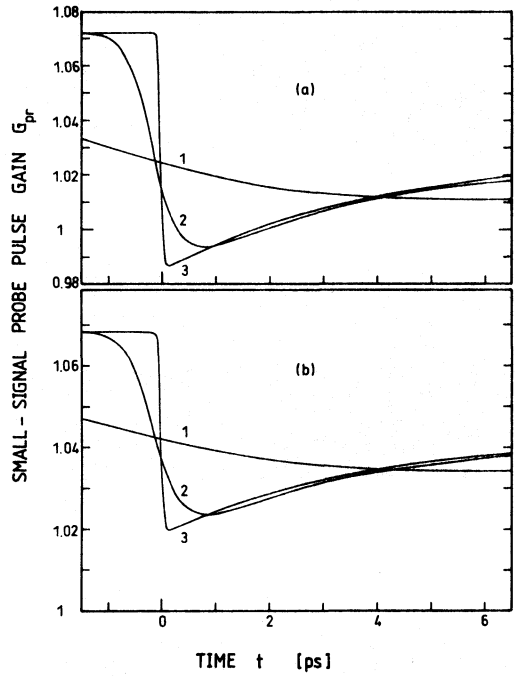

Figure 11 Gain recovery in amplifier jet. The small-signal amplification per pass G_{pr} is plotted versus time. The durations of the circulating laser pulses are (1) Δt_{in} = 10 ps, (2) Δt_{in} = 1 ps and (3) Δt_{in} = 0.1 ps. (a) λ_L = 580 nm and $I_{0L,G} = 0.65 I^G_{sat,s}$. (b) λ_L = 620 nm and $I_{0L,G} = 0.56 I^G_{sat,s}$. The parameters of Fig. 9 and Table 1 are applied.

curvature of gain cavity larger than mirror curvature of absorber cavity). If the circulating pulse is adjusted to the optimum pulse shortening peak intensity $I^{A}_{0L,opt}$ in the absorber jet then the peak intensity $I_{0L,G}$ in the gain jet is far below $I^G_{0L,opt}$ so that the pulse broadening in the amplifier jet is still weak. The optimum pulse shortening per round-trip is already approximately given by the δt_A curves in Fig. 6 (shortening of symmetric Gaussian pulses in saturable absorber).

The reduction of the gain G_{TI} with rising laser intensity stabilizes the laser to a stable steady-state round-trip intensity. Making $t_R/4 < \tau_F$ helps in the intensity stabilization and hinders the creation of additional pulses in the oscillator.

The gain depletion and gain recovery in the gain jet versus time is displayed in Fig. 11 for input pulse durations of 10, 1 and 0.1 ps. The situations at λ_L = 580 nm with $I_{0L,G} = 0.65 I^G_{sat,s}$ and at 620 nm with $I_{0L,G} = 0.56 I^G_{sat,s}$ are shown. The gain reduction is active in the background signal suppression in the temporal region behind the pulse. The partial fast gain recovery behind the pulse is due to the population relaxation out of the lower laser level (1* of Fig. 2c) with the time constant τ_{S0}. After this partial recovery the final gain is recovered by upper laser level population with the pump laser.

3.3. Pulse broadening by group velocity dispersion in gain and absorber jet

The transit time through a sample of thickness l is $t_{tr} = l/v_g = l(n - \lambda \partial n/\partial \lambda)/c_0$ where v_g is the group velocity, n is the phase refractive index, and c_0 is the vacuum light velocity. The transit time is wavelength dependent due to the dispersion of the refractive index. It results in a time-chirp across the spectral width. This transit time spread causes a temporal broadening δt_{tr} of pulses of spectral width $\Delta \nu_L$ and corresponding wavelength width $\Delta\lambda = \lambda_0^2 \Delta \nu_L / c_0$. The temporal broadening is

$$\delta t_{tr} = |t_{tr}(\lambda_0 + \Delta\lambda/2) - t_{tr}(\lambda_0 - \Delta\lambda/2)| \approx \frac{l}{c_0} \lambda_0 \Delta\lambda \left|\frac{\partial^2 n}{\partial \lambda^2}\right| = \frac{l}{c_0^2} \lambda_0^3 \Delta \nu_L \left|\frac{\partial^2 n}{\partial \lambda^2}\right| \quad (19)$$

where λ_0 is the central laser wavelength. The approximation in Equation 19 is obtained by cutting the Taylor expansion of $t_{tr}(\lambda)$ after the first derivative.

The spectral width of the laser is approximately given by

$$\Delta\nu_L \approx [(\Delta\nu_L^{bwl})^2 + (\delta\nu_c)^2]^{1/2} \tag{20}$$

where $\Delta\nu_L^{bwl} = 0.441/\Delta t_L$ [54] is the spectral width of a bandwidth limited Gaussian pulse and $\delta\nu_c$ is the spectral broadening due to self-phase modulation (frequency chirp, see Section 3.6).

The refractive index n and its second derivative $\partial^2 n/\partial\lambda^2$ have contributions from the solvent and the solute. The solvent data n_S [53] and $\partial^2 n_S/\partial\lambda^2$ are given in Fig. 12a and 12c (solid curve), respectively. The solute contribution of the gain and loss medium to n and $\partial^2 n/\partial\lambda^2$ are estimated in the following.

The gain medium contribution Δn_G to the refractive index is given approximately by [55, 56]

$$\begin{aligned}\Delta n_G(\tilde{\nu}) &= \frac{\chi'_G}{2n_S} \approx \frac{\chi''_{G,max}}{4n_S} \frac{(\tilde{\nu}_{G,0} - \tilde{\nu})\Delta\tilde{\nu}^G_{abs}}{(\tilde{\nu}_{G,0} - \tilde{\nu})^2 + (\Delta\tilde{\nu}^G_{abs}/2)^2} \\ &= \frac{\kappa_{G,max}}{2} \frac{(\tilde{\nu}_{G,0} - \tilde{\nu})\Delta\tilde{\nu}^G_{abs}}{(\tilde{\nu}_{G,0} - \tilde{\nu})^2 + (\Delta\tilde{\nu}^G_{abs}/2)^2} \\ &= \frac{N_G\sigma^G_{abs,max}}{8\pi\tilde{\nu}} \frac{(\tilde{\nu}_{G,0} - \tilde{\nu})\Delta\tilde{\nu}^G_{abs}}{(\tilde{\nu}_{G,0} - \tilde{\nu})^2 + (\Delta\tilde{\nu}^G_{abs}/2)^2}\end{aligned} \tag{21}$$

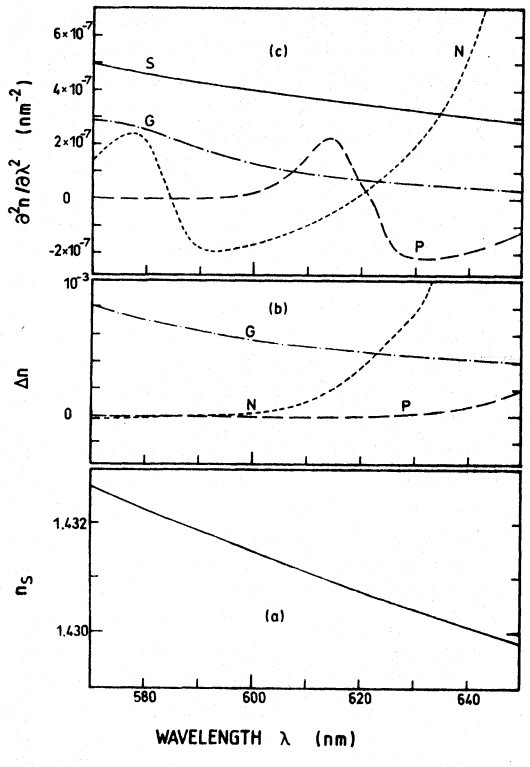

Figure 12 Refractive index data. (a) Refractive index of ethylene glycol at 20°C (from [53]). (b) Refractive index contributions of rhodamine 6G (*G*) and of N-isomer (*N*) and P-isomer (*P*) of DODCI under steady state pumping conditions (*P*-isomer mole fraction given in Fig. 13b). (c) Second derivatives of refractive indices: *S*, solvent $\partial^2 n_S/\partial\lambda^2$. *G*, gain dye $\partial^2\Delta n_G/\partial\lambda^2$. *N*, DODCI *N*-isomer $\partial^2\Delta n_N/\partial\lambda^2$. *P*, DODCI *P*-isomer $\partial^2\Delta n_P/\partial\lambda^2$.

χ'_G and χ''_G are the real and imaginary parts of the linear dye susceptibility. $\kappa_G = \chi''_G/2n_S$ is the extinction coefficient of the dye. κ_G is related to the absorption coefficient α_G and the absorption cross-section σ_G by $\kappa_G = \alpha_G/4\pi\tilde{\nu} = N_G\sigma^G_{abs}/4\pi\tilde{\nu}$ [57]. σ^G_{abs} is plotted in Fig. 8. $\tilde{\nu}_{G,0}$ is the wavenumber of maximum absorption cross-section. $\Delta\tilde{\nu}^G_{abs}$ is the spectral half-width of the absorption spectrum of the gain medium. For the applied dye parameters the calculated Δn_G and $\partial^2\Delta n_G/\partial\lambda^2$ data are plotted in Fig. 12b and c (dash-dotted curves). At 580 nm $\partial^2\Delta n_G/\partial\lambda^2$ of rhodamine 6G is approximately one half of the solvent value while at 620 nm the rhodamine 6G contribution is reduced to one fifth of the solvent value. $\partial^2\Delta n_G/\partial\lambda^2$ is proportional to the amplifier dye concentration. It is advantageous to use the dye concentation as low as possible (e.g. adjustment of the dye concentration to a small-signal pump pulse transmission of T_{pu} (514 nm) = 0.1, giving $N_G \approx 5 \times 10^{17}\,cm^{-3}$ in our case of $l_G = 0.25$ mm).

The refractive index contribution of the saturable absorber DODCI is given by

$$\Delta n_A = \Delta n_N + \Delta n_P \tag{22a}$$

with

$$\Delta n_N = \frac{N_A(1 - x_P)\sigma^N_{abs,max}\Delta\tilde{\nu}^N_{abs}}{8\pi\tilde{\nu}} \frac{\tilde{\nu}_{N,0} - \tilde{\nu}}{(\tilde{\nu}_{N,0} - \tilde{\nu})^2 + (\Delta\tilde{\nu}^N_{abs}/2)^2} \tag{22b}$$

and

$$\Delta n_P = \frac{N_A x_P \sigma^P_{abs,max}\Delta\tilde{\nu}^P_{abs}}{8\pi\tilde{\nu}} \frac{\tilde{\nu}_{P,0} - \tilde{\nu}}{(\tilde{\nu}_{P,0} - \tilde{\nu})^2 + (\Delta\tilde{\nu}^P_{abs}/2)^2} \tag{22c}$$

where Δn_N is the N-isomer contribution and Δn_P is the P-isomer contribution. $\tilde{\nu}_{N,0}$ and $\tilde{\nu}_{P,0}$ are the wavenumbers of maximum N-isomer absorption cross-section, $\sigma^N_{abs,max}$, and maximum P-isomer absorption cross-section, $\sigma^P_{abs,max}$. $\Delta\tilde{\nu}^N_{abs}$ and $\Delta\tilde{\nu}^P_{abs}$ are the corresponding spectral half-widths of the absorption bands. $\sigma^N_{abs}(\lambda)$ and $\sigma^P_{abs}(\lambda)$ together with $\sigma^N_{em}(\lambda)$ and $\sigma^P_{em}(\lambda)$ are plotted in Fig. 13a (from [37] and [58]). The steady-state P-isomer mole fraction x_P is set to $x_{P,th} + 0.4\,(x_{P,max} - x_{P,th})$ according to the results of [34]. $x_{P,max}$ is the maximum obtainable P-isomer mole fraction in the photoisomerization process [37]. $x_P(\lambda)$ is plotted in Fig. 13b.

In the long-wavelength region Δn_N and Δn_P rise strongly because the absorber number density N_A necessary of the small signal transmission T_0 (Equation 9) increases strongly with the decreasing apparent absorption cross-section.

$\Delta n_N(\lambda)$, $\Delta n_P(\lambda)$, $\partial^2\Delta n_N/\partial\lambda^2$, and $\partial^2\Delta n_P/\partial\lambda^2$ are displayed in Fig. 12b and c (dashed curves). The applied dye parameters are given in Fig. 13 ($T_0 = 0.95$). The calculated $\partial^2\Delta n_A/\partial\lambda^2 = \partial^2\Delta n_N/\partial\lambda^2 + \partial^2\Delta n_P/\partial\lambda^2$ at 620 nm is approximately one fifth of the solvent value, and at 580 nm $\partial^2\Delta n_A/\partial\lambda^2$ is nearly one half of the corresponding value of the solvent.

The transit time broadening per round-trip due to the group velocity dispersion in the absorber and gain jet is

$$\delta t_{tr,GVD} = \delta t_{tr,S} + \delta t_{tr,G} + \delta t_{tr,A} \tag{23}$$

$$\approx \frac{\lambda_0^3\Delta\nu_L}{c_0^2}\left(2(l_A + l_G)\frac{\partial^2 n_S}{\partial\lambda^2} + 2l_G\frac{\partial^2\Delta n_G}{\partial\lambda^2} + 2l_A\frac{\partial^2\Delta n_A}{\partial\lambda^2}\right)$$

In Fig. 6 the transit time broadenings $\delta t_{tr,GVD}$ (curves 2 and 2') and $\delta t_{tr,S}$ (curves 1 and 1') for $\Delta\nu_L = \Delta\nu_L^{bwl}$ (no self-phase modulation) and $\delta t_{tr,GVD}$ including self-phase modulation (curves 3 and 3', see below) are shown. Here the situation without self-phase modulation

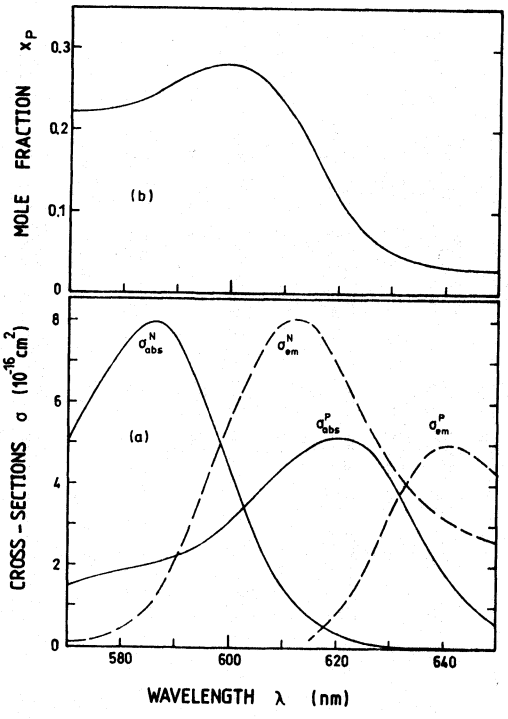

Figure 13 DODCI parameters. (a) Absorption, σ_{abs} and emission, σ_{em}, cross-section spectra of *N*-isomers and *P*-isomers [37, 58]. (b) Steady-state mole fraction of *P*-isomers [34].

is discussed. $\delta t_{tr,G}$ dominates over $\delta t_{tr,A}$ because of $l_G \gg l_A$. The transit time broadening is inverse proportional to the pulse duration. The crossing points of the pulse shortening curves δt_A with the transit time broadening curves $\delta t_{tr,GVD}$ determine approximately the steady-state CPM laser pulse durations, if no additional dispersive elements are included in the resonator (e.g. prism pairs) which counteract the temporal chirp across the spectrum (compensation of group velocity dispersion). For the two examples calculated here (curves 2 and 2′) steady-state pulse durations of Δt_L (620 nm) $\simeq$ 110 fs and Δt_L (580 nm) $\simeq$ 185 fs are obtained. The steady-state pulse duration due to the group-velocity dispersion of the solvent alone would result in pulse durations of 100 fs at 620 nm and 150 fs at 580 nm (crossing of $\delta t_{tr,S}$ with δt_A). Pulse durations of Δt_L (620 nm) $\approx$ 75 fs and Δt_L (580 nm) $\approx$ 130 fs should be obtainable if the total thickness of the gain jet would be reduced to half its value without increasing the amplifier dye concentration.

An increase of the saturable absorber concentration in the loss jet would increase the pulse shortening δt_A per round-trip without a noticeable increasing of $\delta t_{tr,GVD}$ resulting in shorter steady-state pulse durations.

3.4. Finite bandwidth effects of gain medium and absorber medium

The spectral width $\Delta\tilde{\nu}_G$ of laser dyes is typically 1000 to 2000 cm^{-1}. The spectral widths of the pulses is restricted to $\Delta\nu_L \leqslant \Delta\nu_G$ because the amplification is reduced in the spectral wings of the pulses. For bandwidth-limited Gaussian pulses the shortest obtainable pulse duration is limited to $\Delta t_L \geqslant \Delta t_{L,G} = 0.441/\Delta\nu_G$. $\Delta t_{L,G}$ is 15 fs for $\Delta\tilde{\nu}_G \approx 1000$ cm^{-1}.

Chirped pulses having a bandwidth limited spectral width $\Delta\nu_L^{bwl}$ small compared to $\Delta\nu_G$ are compressed by the gain medium because the time shifted spectral wings are less amplified than the pulse centre [59–63].

The spectral width of the saturable absorber medium is similar to the spectral width of the gain medium. The finite spectral width here has a slight pulse shortening effect [64] (spectral wings are less absorbed).

3.5. Finite bandwidth effects of laser mirrors

For CPM lasers broad-band single-stack mirrors are used. The spectral width $\Delta\tilde{\nu}_M$ is typically 2000 to 4000 cm^{-1}. Pulses of duration $\Delta t_L < 1/\Delta\nu_M$ would suffer severe transmission losses. Therefore the mirrors limit durations of circulating pulses in the resonator to $\Delta t_L > \Delta\nu_M^{-1} \approx 10$ fs. For linear chirped pulses with $\Delta\nu_L^{bwl} < \Delta\nu_M$ and $\Delta\nu_L \geqslant \Delta\nu_M$ the mirrors act pulse compressive as in the case of the gain medium [65].

3.6. Self-phase modulation effects

Self-phase modulation occurs due to laser induced refractive index changes [66–69] in the gain and absorber jets. They are due to population changes [4, 40, 70–73] in the saturable absorber (absorber saturation modulation [29–31]) and the gain medium (gain depletion modulation) as well as due to the optical Kerr effect in the solvents [4, 40, 70–82].

The combined frequency chirp (frequency sweep versus time) $\nu_c(t) = \nu(t) - \nu_L$ in the absorber and gain jet per round-trip is given by [41, 42, 83–85]

$$\nu_{c,1}(t) = -\frac{1}{2\pi}\frac{\partial\Delta\phi}{\partial t} = -\frac{1}{2\pi}\frac{\partial}{\partial t}(2\Delta k_G l_G + 2\Delta k_A l_A)$$

$$= -\frac{\nu_L}{c_0}\left(2l_G\frac{\partial}{\partial t}n_G + 2l_A\frac{\partial}{\partial t}n_A\right) \tag{24}$$

$\Delta\phi$ is the phase caused by the refractive index changes. Δk_G and Δk_A are the corresponding wavevector changes. The refractive indices are $n_G(t) = n_S + \Delta n_{K,G}(t) + \Delta n_G(t)$ and $n_A(t) = n_S + \Delta n_{K,A}(t) + \Delta n_A(t)$. $\Delta n_{K,G}(t)$ and $\Delta n_{K,A}(t)$ are the refractive index changes of the solvent in the gain and absorber jet due to the optical Kerr effect.

An up-chirp, i.e. $\partial\nu_c/\partial t > 0$, acts pulse broadening, and a down-chirp, i.e. $\partial\nu_c/\partial t < 0$, acts pulse compressing in a medium with positive group velocity dispersion, $\partial^2 n/\partial\lambda^2 > 0$, as is the case here ($\partial^2 n/\partial\lambda^2 = \partial^2 n_S/\partial\lambda^2 + \partial^2\Delta n_G/\partial\lambda^2 + \partial^2\Delta n_N/\partial\lambda^2 + \partial^2\Delta n_P/\partial\lambda^2$, see Fig. 12c).

The frequency chirp is accumulative in the repetitive transits within the photon lifetime in the resonator. The number of circulations within the resonator photon lifetime is approximately $m_{tr} \approx 1/\ln(R_{out}^{-1})$. The steady-state chirp is approximately

$$\nu_c(t) = \frac{\nu_{c,1}(t)}{\ln(R_{out}^{-1})} \tag{25}$$

The chirp gives a spectral pulse broadening of $\delta\nu_c = \nu_{c,max} - \nu_{c,min}$.

The temporal refractive index changes, the frequency chirps and spectral broadenings are discussed in the following.

3.6.1. Inhomogeneous absorber saturation and gain depletion modulation

The dye absorption spectra (Fig. 8 and Fig. 13a) are determined by inhomogeneously broadened multi-level transitions (excitation of vibronic S_1 states in the case of short-wavelength S_0–S_1 excitation; transitions from vibrationally excited levels in S_0-state to the S_1 band in the case of long-wavelength S_0–S_1 excitation). The gain and absorption

transitions are resonant and occur practically without a refractive index change. Temporal refractive index variations occur due to intra- and interband relaxations after the resonant transitions. In previous investigations [70, 74–78] the S_0–S_1 transitions were considered homogeneously broadened and off-resonance excitation was studied. The transitions may be considered apparently homogeneously broadened for $\Delta t_L > T_3$, τ_{FC}, and τ_{S0}.

The schematic refractive index variation of the dye in the gain jet is illustrated in Fig. 14a. The circulating pulse position is included. Due to c.w. laser pumping at 514 nm the ground-state absorption and correspondingly the refractive index contribution Δn_G are reduced. The circulating laser pulse transfers excited molecules in the S_1-state to a resonant Franck-Condon level (1* in Fig. 2c) in the S_0-state without remarkable refractive index change. The following relaxation from the Franck-Condon level to a thermal ground-state distribution (level 1 of Fig. 2c) leads to a refractive index recovery towards $\Delta n_{G,0}$ with the time constant τ_{S0}. $\Delta n_{G,0}$ is the refractive index contribution of the dye without laser pumping.

The refractive index modulation depth δn_G is given by

$$\delta n_G \approx \frac{|N_2(t_a) - N_2(t_e)|}{N_G} \Delta n_{G,0} = \frac{\ln [G(t_a)] - \ln [G(t_e)]}{l_G \sigma_L N_G} \Delta n_{G,0}$$

$$\approx \frac{G(t_a) - G(t_e)}{G_0} \frac{\Delta n_{G,0}}{l_G \sigma_L N_G} \tag{26}$$

where $G_0 = (R_{out}^{1/2} T_0)^{-1}$ is the initial small-signal gain. The time positions t_a and t_e before and behind the circulating pulse are indicated in Fig. 14a. $G(t_a) - G(t_e)$ is considerably smaller than G_0 since the gain depletion is made small to avoid pulse broadening (see Figs 9 and 10).

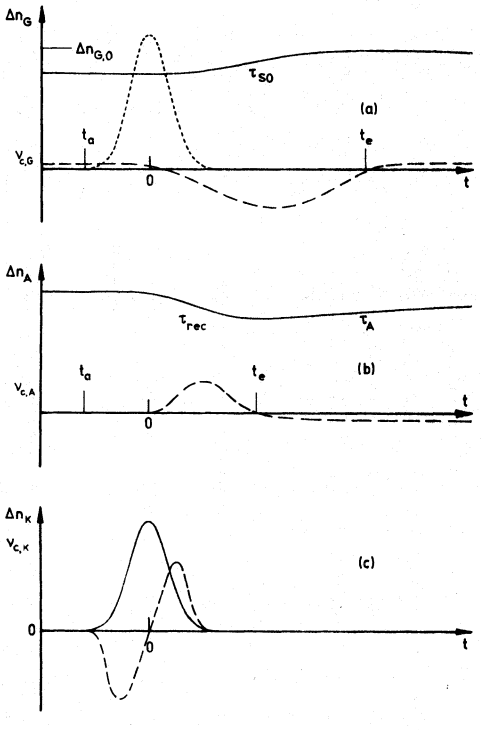

Figure 14 Illustration of temporal refractive index changes and frequency chirps. (a) Refractive index change (——) and frequency chirp (- - -) due to gain jet pumping and gain depletion. (- - -) curve indicates shape and position of circulating laser pulse. (b) Refractive index change (——) and frequency chirp (- - -) due to saturable absorption in loss jet. Situation at λ_L = 620 nm is shown (at 580 nm signs reverse). (c) Refractive index change (——) and frequency chirp (- - -) caused by electronic Kerr effect of solvent.

The chirp contribution, $\nu_{c,G} = -\tilde{\nu}_L 2l_G(\partial\Delta n_G/\partial t)/\ln(R_{out}^{-1})$, is indicated by the dashed curve in Fig. 14a. A down- and up-chirp occurs behind the pulse while the pulse itself is nearly unchirped in the case of $\tau_{S0} > \Delta t_L$.

The modulation depth of the frequency chirp is approximately given by

$$\delta\nu_{c,G} \approx \frac{\tilde{\nu}_L 2l_G \delta n_G}{\tau_{S0} \ln(R_{out}^{-1})} \tag{27}$$

for $\Delta t_L < \tau_{S0}$. The ratio of total frequency sweep $\delta\nu_{c,G}$ to the bandwidth-limited spectral width of the circulating pulse, $\Delta\nu_L^{bwl} = 0.441/\Delta t_L$, is

$$\frac{\delta\nu_{c,G}}{\Delta\nu_L^{bwl}} \approx \begin{cases} \dfrac{2l_G\tilde{\nu}_L\delta n_G}{0.441\ln(R_{out}^{-1})}\dfrac{\Delta t_L}{\tau_{S0}} & \text{for } \Delta t_L < \tau_{S0} \quad (28a) \\ \dfrac{2l_G\tilde{\nu}_L\delta n_G}{0.441\ln(R_{out}^{-1})} & \text{for } \Delta t_L > \tau_{S0} \quad (28b) \end{cases}$$

For $\Delta t_L < \tau_{S0}$ and parameters of Table 1 and Fig. 12 the ratios are $\delta\nu_{c,G}(580\,\text{nm})/\Delta\nu_L^{bwl} \approx 0.48\,[G(t_a) - G(t_e)]\Delta t_L/\tau_{S0}G_0$ and $\delta\nu_{c,G}(620\,\text{nm})/\Delta\nu_L^{bwl} \approx 0.76\,[G(t_a) - G(t_e)]\Delta t_L/\tau_{S0}G_0$. The ratio $\delta\nu_{c,G}/\Delta\nu_L^{bwl}$ is small and it has no influence on short pulses ($\Delta t_L < \tau_{S0}$) because then the chirp occurs behind the pulse.

The refractive index variation of the absorber dye versus time is illustrated in Fig. 14b. The circulating laser pulse transfers molecules resonantly from S_0 to S_1 without appreciable change of refractive index. The following relaxation from the Franck-Condon state in the S_1-band with the time constant τ_{FC} in the case of short-wavelength excitation (N- and P-isomers at 580 nm), or the following redistribution in the S_0 ground-state with the spectral cross-relaxation time T_3 in the case of long-wavelength excitation (N-isomer at 620 nm) changes the refractive index contribution Δn_A. It recovers to the initial value $\Delta n_{A,0}$ with the absorption recovery time constants τ_N for the N-isomers and τ_P for the P-isomers.

The refractive index modulation depth δn_A is approximately given by

$$\delta n_A = \delta n_N + \delta n_P \approx (\Delta n_N \rho_N + \Delta n_P)\frac{T(t_e) - T(t_a)}{1 - T_0} \tag{29}$$

ρ_N gives the fraction of N-isomers interacting with the circulating laser pulse. ($\rho_N = 1$ in the case of short-wavelength excitation; for long-wavelength excitation ρ_N is given by Equation 8).

The frequency chirp contribution $\nu_{c,A}$ is indicated by the dashed curve in Fig. 14b. It is given by $\nu_{c,A} = -\tilde{\nu}_L 2l_A(\partial\Delta n_A/\partial t)/\ln(R_{out}^{-1})$. An up-chirp and down-chirp occur behind the pulse while the pulse itself is nearly unchirped in the case of $\Delta t_L < \tau_{rec}$, where τ_{rec} is either τ_{FC} or T_3 depending on short-wavelength or long-wavelength interaction.

The ratio of the total frequency sweep $\delta\nu_{c,A}$ to the bandwidth limited spectral pulse width $\Delta\nu_L^{bwl}$ is

$$\frac{\delta\nu_{c,A}}{\Delta\nu_L^{bwl}} \approx \begin{cases} \dfrac{2l_A\tilde{\nu}_L\delta n_A}{0.441\ln(R_{out}^{-1})}\dfrac{\Delta t_L}{\tau_{rec}} & \text{for } \Delta t_L < \tau_{rec} \quad (30a) \\ \dfrac{2l_A\tilde{\nu}_L\delta n_A}{0.441\ln(R_{out}^{-1})} & \text{for } \Delta t_L > \tau_{rec} \quad (30b) \end{cases}$$

For $\Delta t_L < \tau_{rec}$ and the data of Table 1 and Fig. 12 one calculates $\delta\nu_{c,A}$ (580 nm)/$\Delta\nu_L^{bwl} \approx 0.12[T(t_e) - T(t_a)]\Delta t_L/(1 - T_0)\tau_{rec}$ and $\delta\nu_{c,A}$ (620 nm)/$\Delta\nu_L^{bwl} \approx 0.18[T(t_e) - T(t_a)]\Delta t_L/(1 - T_0)\tau_{rec}$. The ratio $\delta\nu_{c,A}/\Delta\nu_L^{bwl}$ is small and has no influence for short pulses ($\Delta t_L < \tau_{rec}$). There is a down-chirp at 580 nm and an up-chirp at 620 nm immediately following the pulse.

If the absorber jet is detuned out of the centre position of the resonator, the trailing refractive index recovery behind one pulse causes a frequency chirp on the other delayed counter-propagating pulse. But the above estimates show that the chirp and spectral broadening by the absorber saturation are negligibly small.

3.6.2. Self-phase modulation induced by optical Kerr effect

In the solvent ethylene glycol the refractive index is changed by the optical Kerr effect [86]. On a subpicosecond time scale the electronic Kerr effect contribution is dominant since the response time of the molecular orientation contribution $\tau_{or} \approx 4\pi r^3\eta/3k_B\theta$ (Debye-Stokes-Einstein relation [87]) is of the order of 100 ps, (viscosity $\eta = 19.9$ cP [88], molecular radius $r \approx 0.19$ nm, k_B is the Boltzmann constant, and θ is the temperature).

The electronic refractive index change is given by [66–69, 89]

$$\Delta n_K(t) = \frac{n_2}{n_L \varepsilon_0 c_0} I_L(t) \tag{31}$$

For ethylene glycol a value of $n_2 = 8 \times 10^{-23}\,m^2\,V^{-2}$ is given in [7, 48, 72, 78, 79] for the field coefficient of the nonlinear refractive index. n_L is the linear refractive index at the laser frequency, ε_0 is the permittivity, and c_0 is the vacuum light velocity. $\Delta n_K(t)$ is illustrated by the solid curve in Fig. 14c. It has the same temporal shape as the laser pulse.

The accumulated frequency chirp due to the Kerr effect (Equations 24 and 25) is given by

$$\nu_{c,K}(t) = -\frac{\nu_L n_2}{c_0^2 n_L \varepsilon_0 \ln(R_{out}^{-1})}\left(2l_G\frac{A_A}{A_G} + 2l_A\right)\frac{\partial I_{L,A}}{\partial t} \tag{32}$$

A_A/A_G is the ratio of the laser beam cross-sections in the absorber jet and the gain jet. A_A/A_G is equal to $I_{L,G}/I_{L,A}$ the ratio of the laser intensities in the gain and absorber jet. In our experimental arrangement it is $A_A/A_G \approx 0.25$.

$\nu_{c,K}(t)$ is illustrated in Fig. 14c. The pulse is up-chirped in the main intensity part causing a temporal pulse broadening by the normal refractive index dispersion in the gain and absorber jet.

The total spectral broadening ratio due to the Kerr effect is

$$\frac{\delta\nu_{c,K}}{\Delta\nu_L^{bwl}} = \frac{\nu_{c,K,max} - \nu_{c,K,min}}{\Delta\nu_L^{bwl}} = \frac{2^{1/2}4(\ln 2)^{1/2}\tilde{\nu}_L n_2 I_{0L,A}\exp(-1/2)}{0.441 c_0 n_L \varepsilon_0 \ln(R_{out}^{-1})}\left(2l_G\frac{A_A}{A_G} + 2l_A\right) \tag{33}$$

In Equation 33 $\partial I_{L,A}/\partial t|_{max} - \partial I_{L,A}/\partial t|_{min} = 2^{1/2}4(\ln 2)^{1/2} I_{0L,A}\exp(-1/2)/\Delta t_L$ for a Gaussian pulse is used [89]. For optimum pulse shortening $I_{0L,A}$ is given by $I_{0L,opt}^{A}$ of Fig. 5 which is inversely proportional to Δt_L. For $I_{0L,opt}^{A} = 7 \times 10^9\,W\,cm^{-2}$ at $\Delta t_L = 100$ fs and $A_A/A_G = 0.25$ the spectral broadening is $\delta\nu_{c,K}/\Delta\nu_L^{bwl} \approx 1.3$. For our parameters the spectral broadening in the gain jet dominates by a factor of 1.8.

The temporal pulse broadening due to the frequency up-chirp is included in Equation 23 where $\Delta\nu_L$ is given by Equation 20. The total transit time broadening due to the self-phase modulated spectral pulse width is shown by the curves 3 and 3′ in Fig. 6. The total transit time broadening limits the obtainable pulse duration to ≈ 150 fs at 620 nm and to ≈ 230 fs at 580 nm. Reducing the gain jet thickness a factor of two leads to $\Delta t_L \approx 110$ fs at 620 nm and $\Delta t_L \approx 170$ fs at 580 nm. Pulse durations below these limits may be achieved by using higher saturable absorber concentrations, by compensation of the group velocity dispersion, and by pulse compression of the frequency chirped pulses.

3.7. Compensation of group velocity dispersion and pulse compression

The temporal broadening (temporal chirp) of pulses by group velocity dispersion in the gain and absorber jets may be compensated by dispersion elements (removal of temporal chirp) like prism pairs in linear resonators [7, 90, 91], prism quadrupoles in linear [92–95] and ring resonators [10–12, 96–99], Gires–Tournois interferometers [50, 51, 100], frequency off-centre dielectric mirrors [48, 49], (dielectric mirrors act like interferometers and cause frequency dependent propagation changes [101–103]), and combinations of one [104, 105], two [106] and four prisms [107, 108] with a tilted mirror. Additionally the self-phase modulated (frequency chired) pulses may be compressed temporally by the dispersive elements [42, 85]. Pulse durations down to 20 fs have been achieved by appropriate intracavity compensation and compression [10, 11].

3.8. Influence of lateral loss jet detuning

In the linear CPM laser configuration the loss jet has to be centred exactly to the middle position of the resonator in order that the counter-propagating pulses collide in the jet, while in the generally applied ring CPM laser configuration the pulses collide automatically in the saturable absorber jet.

The absorber jet detuning is indicated by the dotted bar in Fig. 1a. The counter-circulating pulses are thought to collide further at the centre of resonator. In this case the pulses pass symmetrically through the absorber as is illustrated in Fig. 1d. An asymmetric circulation, where alternatively the pulses collide and are time separated in the absorber jet, is thought to be unfavourable, because one of the circulating pulses is preferentially absorbed. In the experiments no different pulse heights between adjacent pulses were observed in the case of small length detuning.

The double passages through the absorber within one resonator round-trip are simulated. The calculations are carried out for $\lambda_L = 620$ nm. The saturable absorber equations 1–7 are modified by replacing κI_L by $I_{L,c} + I_{L,cc}$ with appropriate time position shifts. $I_{L,c}$ is the intensity of the clockwise rotating pulse, and $I_{L,cc}$ is the intensity of the counter-clockwise rotating pulse (Fig. 1a).

The time-integrated double-pass transmission $T_{11,2}$ and the double-pass pulse shortening ratio $\beta_{A,2}$ versus time shift δt are displayed in Fig. 15a and b, respectively. The absorber parameters are taken from Table 1 ($T_0 = 0.95$, $\lambda_L = 620$ nm). The input pulse duration is set to $\Delta t_{L,in} = 0.1$ ps and the peak pulse intensity is choosen to be $I_{01,c} = I_{01,cc} = I_{01,opt}^{A}$ ($\delta t = 0$) $= 7 \times 10^9$ W cm^{-2}. The solid curves belong to the experimental situation of $T_3 = 1$ ps (assumed) and $\tau_{FC} = 0.95$ ps [109]. The transmission reduces with increasing δt because of the partial absorption recovery with the time constant τ_{rec} ($= T_3$ or τ_{FC}).

The pulse shortening in the saturable absorber is reduced because per passage only the leading pulse is shortened reasonably while the delayed pulse passes through a bleached

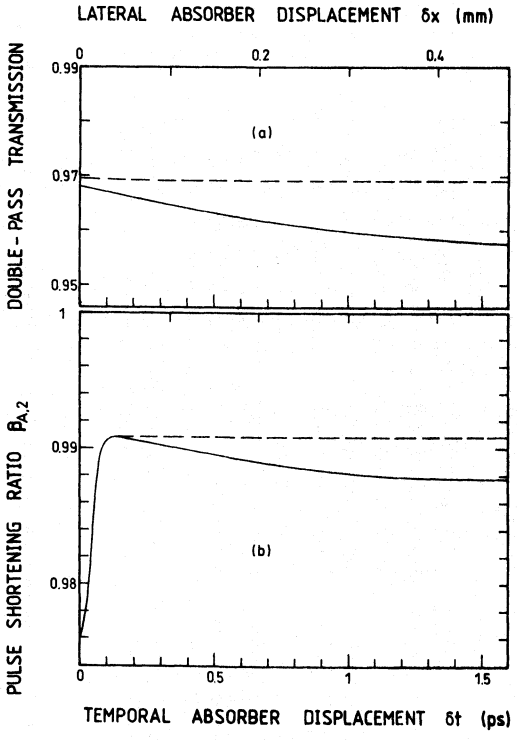

Figure 15 Influence of lateral absorber jet displacement on time-integrated round-trip transmission through saturable absorber (a) and on pulse shortening (b). The absorber and resonator parameters of Table 1 are applied with $\lambda_L = 620\,\text{nm}$, $\Delta t_{L,in} = 0.1\,\text{ps}$ and $I_{0L,A} = 7 \times 10^9\,\text{W cm}^2$. (——) curves, $T_3 = 1\,\text{ps}$ and $\tau_{FC} = 0.95\,\text{ps}$. (- -) curves, $T_3 = \tau_{FC} = 10\,\text{ns}$.

dye. The increasing pulse-shortening for $\Delta t_L < \delta t \leqslant \tau_{rec}$ is due to the partial absorption recovery.

The dashed curves of Fig. 15a and b illustrate the situation for $T_3 = \tau_{FC} = 10\,\text{ns}$. Without the partial absorption recovery the transmission remains constant and no change of pulse shortening is observed for $\delta t > \Delta t_L$ is the displayed time-shift region.

Besides the reduced pulse shortening in the saturable dye due to temporal pulse separation the transit time broadening due to the self-phase modulation induced by the optical Kerr effect in the absorber jet is reduced because of intensity reduction. Both effects may compensate so that the pulse duration is not influenced by the temporal overlap in the absorber jet. Experimental results are reported in [7].

4. Pulse development in multiple resonator round-trips

In Section 3 the pulse shortenings and pulse broadenings in one resonator round-trip were analysed to get an estimate of the steady-state pulse duration in a CPM rhodamine 6G-DODCI dye laser. In this section multiple resonator round-trips are simulated in order to get information about the influence of the partial fast dye recoveries (T_3, τ_{FC}, τ_{S0}) and of the laser focusing ratio $I_{L,G}/I_{I,A}$ on the background signal suppression and temporal pulse shaping.

In the calculations it is assumed that the absorber transmission recovers completely to the small-signal transmission value before the next pulse passage, and that the c.w. pump laser keeps the circulating pulse energy constant. The necessary upper laser level population is

$$N_{2,0} = \frac{\ln (T_{TI}^{-1} R_{out}^{-1/2})/l_G + N_G \sigma_W}{\sigma_L + \sigma_W} \tag{34}$$

and the pump laser intensity I_{pu} is derived from the relation

$$N_{2,0} = \frac{I_{pu}\tau_F}{h\nu_L I_G}\left[1 - \exp\left(-\frac{t_R}{4\tau_F}\right)\right]\left[1 - \exp\left(-\sigma_{pu}N_G l_G\right)\right] \tag{35}$$

The temporal development of an initially symmetric Gaussian pulse with a constant background signal level in multiple round-trips through the CPM oscillator is investigated (considered temporal region is $-5t_0 < t < 15t_0$ where t_0 is the initial pulse width).

In Fig. 16 the resulting pulse shapes after 100 round-trips are shown. The dye and resonator parameters of Table 1 are applied ($\lambda_L = 620$ nm). The initial pulse shape is shown by the dotted curve. The initial background signal height is $I_B = 0.01\, I_{0L}$. The partial recovery times are set to $T_3 = 1$ ps (assumed), $\tau_{FC} = 0.95$ ps [109], and $\tau_{S0} = 4$ ps [110]. The initial pulse duration is set to $\Delta t_L = 1$ ps and the initial peak intensity is choosen to be $I_{0L,A} = I^{A}_{0L,opt}$ ($= 7 \times 10^8$ W cm^{-2}, see Fig. 5). Curves 1–4 belong to different intensity focusing ratios $I_{0L,G}/I_{0L,A}$. The background suppression in the trailing part of the pulse and the temporal pulse width vary with focusing ratio.

The optimum background suppression $I_{L,min}/I_B$ and the accumulated pulse shortening ratio $\Delta t_L(100)/\Delta t_L(0)$ versus intensity focusing ratio are shown in Fig. 18 (solid curves). Below $I_{0L,G}/I_{0L,A} = 0.1$ the background suppression and the pulse shortening ratio remain practically constant. At $I_{0L,G}/I_{0L,A} = 4$ (i.e. $I_{0L,G}I^{A}_{sat,s}/I_{0L,A}I^{G}_{sat,s} = S^{-1} \approx 0.5$ where S is New's stability parameter [13, 20]) there is a slight minimum. For larger focusing ratios ($I_{0L,G}/I_{0L,A} > 10$, $S < 0.8$) no build-up of a femtosecond pulse train is possible (no background suppression and pulse shortening).

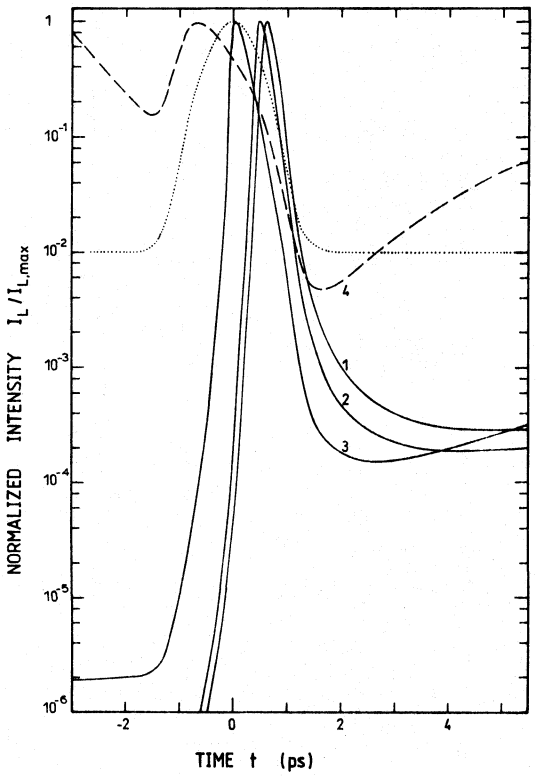

Figure 16 Temporal pulse shapes after 100 resonator round-trips. Initial pulse shape is shown by (····) curve. Dye and resonator parameters are given in Table 1. Laser wavelength is λ_L = 620 nm (T_3 = 1 ps, τ_{FC} = 0.95 ps, τ_{S0} = 4 ps). The intensity focusing parameters are $I_{0L,G}/I_{0L,A}$ = 0.1 (1), 1 (2), 5 (3) and 10 (4).

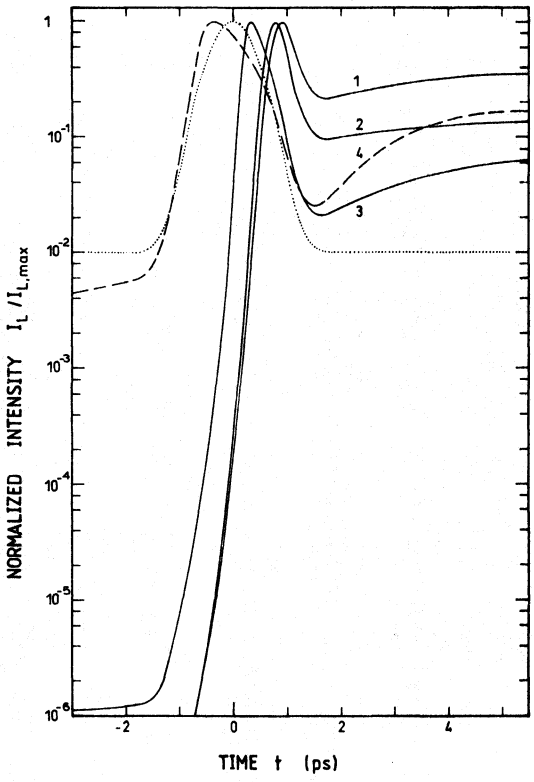

Figure 17 Temporal pulse shapes after 100 resonator round-trips in the case of no fast partial absorption recovery. The curves belong to the same parameters as in Fig. 16 except $T_3 = \tau_{FC} = 10$ ns.

The intensity rise in the trailing pulse region of Fig. 16 is due to the finite relaxation time τ_{S0} (= 4 ps) of the lower laser level of the gain dye. The gain recovers partially due to the depopulation of the lower laser level.

The importance of a fast partial absorption recovery is seen by comparing the curves of Fig. 17 with the curves of Fig. 16. The parameters are the same except $T_3 = \tau_{FC} = 10$ ns. For all intensity focusing parameters in Fig. 17 there is no background suppression but background amplification ($I_{L,min}/I_B > 1$) in the trailing part of the pulse. This behaviour makes a femtosecond pulse train formation starting from the spontaneous emission in the gain jet impossible. This situation is also seen by the dashed curves in Fig. 18.

In the analysis of the pulse shortening action of the saturable dye DODCI in multiple transits [34] the necessity of a fast partial absorption recovery for background suppression was already shown. Since the gain medium mainly causes pulse broadening (see Fig. 10) the necessary condition of a fast partial absorption recovery for background suppression remains valid for the complete CPM laser with absorption saturation and gain depletion. The application of a slow saturable absorber (S_1–S_0 relaxation time $\tau_A > \Delta t_L$; τ_A stands for τ_N and τ_P in the case of DODCI) is necessary to have a low enough fast saturation intensity $I^A_{sat,f}$ to start bleaching and passive mode-locking. $I^A_{sat,f}$ is given by [34]

$$I^A_{sat,f} = \frac{h\nu_L}{\tau_N \rho_N (1 - x_{P,th}) + \tau_P x_{P,th}} \left[\frac{\rho_N (1 - x_{P,th})}{\sigma_N} + \frac{x_P}{\sigma_P} \right] \tag{36}$$

The use of a photoisomer forming absorber with absorption increase by photoisomerization (for $\lambda_L > 607$ in the case of DODCI dissolved in ethylene glycol, see Fig. 13) is advantageous

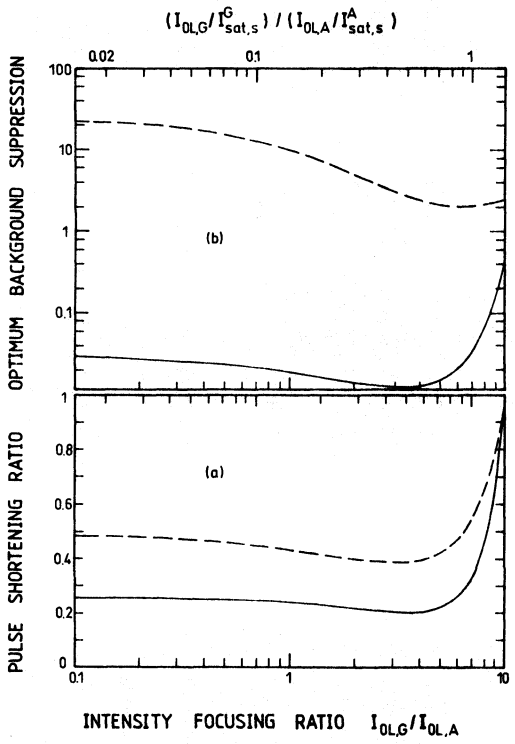

Figure 18 Accumulated pulse shortening ratio $\Delta t_L(100)/\Delta t_L(0)$ (a) and optimum background suppression $I_{L,min}(100)/I_n$ (b) after 100 round trips. (——) curves apply to parameters of Fig. 16 (T_3 = 1 ps, τ_{FC} = 0.95 ps). (– –) curves apply to parameters of Fig. 17 ($T_3 = \tau_{FC}$ = 10 ns).

because of low lasing threshold (initial T_0 is high) and enhanced steady-state pulse shortening (absorption increase). Additionally the higher isomer absorption leads to a lower steady-state intensity in the gain jet because less gain depletion is needed to keep the circulating pulse energy at a constant value.

5. Conclusions

The femtosecond pulse development in a CPM dye laser was studied. Especially the rhodamine 6G-DODCI gain–loss combination was simulated. The steady-state pulse duration was estimated by the balance of pulse shortening and pulse broadening in one resonator round-trip.

The pulse shortening was found to be due to the saturable absorber action, and the pulse broadening was found to be caused by the group velocity dispersion of the self-phase modulated pulses in the resonator. The self-phase modulation (frequency chirp) of the femtosecond pulses was shown to be caused by the electronic optical Kerr effect of ethylene glycol in the gain and absorber jet ($\propto \partial n/\partial t$), while the inhomogeneous absorber saturation and gain depletion practically do not contribute on a femtosecond time scale. The pulse broadening (transit time broadening) due to the group velocity dispersion ($\propto \partial^2 n/\partial\lambda^2$) was dominated by the contribution of ethylene glycol in the gain and loss jets (transit time broadening is proportional to jet thickness).

Without compensation of group velocity dispersion and without intracavity pulse compressions the calculations determine minimum obtainable pulse durations of about 100 fs at 620 nm for an absorber small signal transmission of T_0 = 0.95. Shorter durations require a compensation of the group velocity dispersion and a temporal compression of the frequency chirped pulses in the resonator by either prisms, interferometers, or mirrors.

In the simulation of multiple resonator round-trips it was shown that a fast partial absorption recovery (time constant in the 0.1 ps to 10 ps time range) of the slow saturable absorber (total absorption recovery time τ_A around 1 ns, $\tau_A \ll t_R/2$) is necessary for femtosecond pulse train formation. The fast partial absorption recovery leads to background signal suppression which is needed to form a femtosecond pulse train out of the fluorescence emission of the gain dye.

The gain depletion in the amplifier jet was found to have mainly a pulse broadening effect. The normalized intensity ratio $(I_{0L,G}/I^{G}_{sat,s})/(I_{0L,A}/I^{A}_{sat,s}) = S^{-1}$ between the gain jet intensity and the absorber jet intensity has to be kept below 1 (optimum value is $S^{-1} = 0.5$) to achieve pulse shortening and background signal suppression in the evolution to a steady-state femtosecond pulse train.

References

1. R. L. FORK and C. V. SHANK, *Appl. Phys. Lett.* **38** (1981) 671.
2. C. V. SHANK, in 'Ultrashort Laser Pulses and Applications', edited by W. Kaiser, Top. in Appl. Phys. **60** (Springer-Verlag, Berlin, 1988) p.5.
3. A. PENZKOFER, *Appl. Phys.* **B46** (1988) 43.
4. J. C. DIELS, in 'Dye Laser Principles with Applications', edited by F. J. Duarte and L. W. Hillman (Academic Press, Boston, 1990) p. 41.
5. J. C. DIELS, N. JAMASBI and L. SARGER, in 'Ultrafast Phenomena V', edited by G.R. Fleming and A. E. Siegman (Springer-Verlag, Berlin, 1986) p.2.
6. I. S. RUDDOCK and D. J. BRADLEY, *Appl. Phys. Lett.* **29** (1976) 296.
7. W. BÄUMLER and A. PENZKOFER, *Opt. Quantum Electron.* to be published.
8. P. M. W. FRENCH and J. R. TAYLOR, *Opt. Letters* **13** (1988) 470.
9. M. D. DAWSON, T. F. BOGGERS, D. W. GARVEY and A. SMIRL, *IEEE J. Quantum. Electron.* **QE-23** (1987) 290.
10. J. A. VALDMANIS and R. L. FORK, *IEEE J. Quantum. Electron.* **QE-22** (1986) 112.
11. A. FINCH, G. CHEN, W. SLEAT and W. SIBBETT, *J. Mod. Optics* **35** (1988) 345.
12. J. A. VALDMANIS, R. L. FORK and J. P. GORDON, *Opt. Letters* **10** (1985) 131.
13. G. H. C. NEW, *IEEE J. Quantum Electron.* **QE-10** (1974) 115.
14. G. H. C. NEW and D. H. REA, *J. Appl. Phys.* **47** (1976) 3107.
15. B. K. GARSIDE and T. K. LIM, *J. Appl. Phys.* **44** (1973) 2335.
16. T. K. LIM and B. K. GARSIDE, *Opt. Commun.* **12** (1974) 8.
17. H. A. HAUS, *IEEE J. Quantum Electron.* **QE-11** (1975) 736.
18. J. HERRMANN, J. WEIDNER and B. WILHELMI, *Appl. Phys.* **B26** (1981) 197.
19. J. HERRMANN and J. WEIDNER, *Appl. Phys.* **B27** (1982) 105.
20. M. S. STIX and E. P. IPPEN, *IEEE J. Quantum Electron.* **QE-19** (1983) 520.
21. D. KÜHLKE, W. RUDOLPH and B. WILHELMI, *IEEE J. Quantum Electron.* **QE-19** (1983) 526.
22. W. RUDOLPH and B. WILHELMI, *Appl. Phys.* **B35** (1984) 37.
23. O. E. MARTINEZ, R. L. FORK and J. P. GORDON, *Opt. Letters* **9** (1984) 156.
24. D. KÜHLKE and W. RUDOLPH, *Opt. Quntum Electron.* **16** (1984) 57.
25. O. E. MARTINEZ, R. L. FORK and J.P. GORDON, *J. Opt. Soc. Am.* **B2** (1985) 753.
26. H. A. HAUS and Y. SILBERBERG, *IEEE, J. Quantum. Electron.* **QE-22** (1986) 325.
27. M. S. STIX, *Opt. Letters* **10** (1985) 279.
28. V. PETROV, W. RUDOLPH and B. WILHELMI, *Revue Phys. Appl.* **22** (1987) 1639.
29. H. AVRAMOPOULOS, P. M. W. FRENCH, J. A. R. WILLIAMS, G. H. C. NEW and J. R. TAYLOR, *IEEE J. Quantum Electron.* **QE-24** (1988) 1884.
30. H. AVRAMOPOULOS and G. H. C. NEW, *Opt. Commun.* **71** (1989) 370.
31. H. AVRAMOPOULOS, P. M. W. FRENCH, G. H. C. NEW, M. M. OPALINSKA J. R. TAYLOR and J. A. R. WILLIAMS, *IEEE J. Quantum Electron.* **QE-25** (1989) 2469.
32. H. A. HAUS and M. N. ISLAM, *IEEE J. Quntum Electon.* **QE-21** (1985) 1172.
33. W. L. NIGHAN JR., T. GONG and P. M. FAUCHET, *IEEE J. Quantum Electron.* **QE-25** (1989) 2476.
34. A. PENZKOFER and W. BÄUMLER, *Opt. Quantum Electron.* **23** (1991) 439.

35. A. PENZKOFER, W. FALKENSTEIN and W. KAISER, *Chem. Phys. Letters* **44** (1976) 82.
36. S. DÄHNE, D. LEUPOLD and H. STIEL, *Acta Phys. Polon.* **A71** (1987) 777.
37. W. BÄUMLER and A. PENZKOFER, *Chem. Phys.* **142** (1990) 431.
38. W. BLAU, W. DANKESREITER and A. PENZKOFER, *Chem. Phys.* **85** (1984) 473.
39. A. PENZKOFER and P. SPERBER, *Chem. Phys.* **88** (1984) 309.
40. A. E. SIEGMAN, 'Lasers' (Oxford University Press, Oxford, 1986) Ch. 9.
41. A. M. JOHNSON and C. V. SHANK, in 'The Supercontinuum Laser Source', edited by R. R. Alfano (Springer-Verlag, New York, 1989) p. 399.
42. W. RUDOLPH and B. WILHELMI, 'Light Pulse Compression' (Harwood, London, 1989).
43. R. L. FORK, O. E. MARTINEZ and J. P. GORDON, *Opt. Letters* **9** (1984) 150.
44. J. P. GORDON and R. L. FORK, *Opt. Letters* **9** (1984) 153.
45. W. DIETEL, J. J. FONTAINE and J. C. DIELS, *Opt. Letters* **8** (1983) 4.
46. Z. BOR, *J. Mod. Optics* **35** (1988) 1907.
47. F. J. DUARTE, *Opt. Quantum Electron.* **22** (1990) 467.
48. M. YAMASHITA, M. ISHIKAWA, K. TORIZUKA and T. SATO, *Opt. Letters* **11** (1986) 504.
49. M. YAMASHITA, K. TORIZUKA and T. SATO, *IEEE J. Quantum Electron.* **QE-23** (1987) 2005.
50. J. HEPPNER and J. KUHL, *Appl. Phys. Lett.* **47** (1985) 453.
51. D. KÜHLKE, T. BONKHOFER and D. VON DER LINDE, *Opt. Commun.* **59** (1986) 208.
52. G. GRÖNNINGER and A. PENZKOFER, *Opt. Quantum Electron.* **16** (1984) 225.
53. M. J. TIMMERMANS and MME. HENNAUT-ROLAND, *J. de Chim. Phys.* **32** (1935) 501.
54. E. P. IPPEN and C. V. SHANK, in 'Ultrashort Light Pulses', edited by S. L Shapiro, *Topic in Appl. Phys.* Vol. 18 (Springer-Verlag, Berlin, 1977) p. 83.
55. P. SPERBER, W. SPANGLER, B. MEIER and A. PENZKOFER, *Opt. Quantum Electron.* **20** (1988) 395.
56. M. A. VASIL'EVA, J. VISHCHAKAS, V. GULBINOS, V. I. MALYSHEV, A. V. MASALOV, V. KABELKA and V. SYRUS, *IEEE J. Quantum Electron.* **QE-19**(1983) 724.
57. Y. LU and A. PENZKOFER, *Appl. Optics* **25** (1986) 221.
58. W. BÄUMLER and A. PENZKOFER, *Chem. Phys.* **140** (1990) 75.
59. H. NATHEL, D. M. GUTHALS and J. M. CLARK, Conference on Lasers and Electro-Optics CLEO (June 1984) Anaheim, CA. Paper THI44.
60. D. VON DER LINDE and A. M. MALVEZZI, *Appl. Phys.* **B37** (1985) 1.
61. P. SPERBER and A. PENZKOFER, *Opt. Commun.* **54** (1985) 160.
62. J. SCHMIDT, F. REIL and A. PENZKOFER, *Opt. Commun,* **58** (1986) 427.
63. T. TOMIE, *Jap. J. Appl. Phys.* **24** (1985) 1008.
64. E. YABLONOVICH, *IEEE J. Quantum Electron* **QE-11** (1975) 789.
65. A. S. L. GOMES, A. S. GOUVEIA-NETO, J. R. TAYLOR, H. AVRAMOPOULOS and G. H. C. NEW, *Opt. Commun.* **59** (1986) 399.
66. F. SHIMIZU, *Phys. Rev. Letters* **19** (1967) 1067.
67. S. A. AKHMANOV, R. V. KHOKHLOV and A. P. SUKHORUKOV, in 'Laser Handbook' Vol. 2. edited by F. T. Arecchi and E. O. Schulz-DuBois (North-Holland, Amsterdam, 1972) Ch. E3, p. 1151.
68. Y. R. SHEN, 'The Principles of Nonlinear Optics' (Wiley, New York, 1984).
69. Y. R. SHEN and G. Z. YANG, in 'The Supercontinuum Laser Source', edited by R. R. Alfano (Springer-Verlag, New York, 1989) p. 1.
70. S. DE SILVESTRI, P. LAPORTA and O. SVELTO, *IEEE J. Quantum Electron.* **QE-20** (1984) 533.
71. J. C. DIELS, J. J. FONTAINE, I. C. McMICHAEL and F. SIMONI, *Appl. Opt.* **24** (1985) 1270.
72. Y. ISHIDA, K. NAGANUMA and T. YAJIMA, *IEEE J. Quantum Electron.* **QE-21** (1985) 69.
73. P. HEIST, W. RUDOLPH and V. PETROV, *Appl Phys.* **B49** (1989) 113.
74. O. E. MARTINEZ, R. L. FORK and J. P. GORDON, *J. Opt. Soc. Am.* **B2** (1985) 753.
75. J. C. DIELS, W. DIETEL, J. J. FONTAINE, W. RUDOLPH and B. WILHELMI, *J. Opt. Soc. Am.* **B2** (1985) 680.
76. B. WILHELMI, R. RUDOLPH, E. DÖPEL and W. DIETEL, *Optica Acta* **32** (1985) 1175.
77. B. WILHELMI, *Annalen der Physik, 7. Folge*, Band **43** (1986) 355.
78. R. S. MIRANDA, G. R. JACOBOVITZ, C. H. BRITO CRUZ and M. A. F. SCARPARO, *Opt. Letters* **11** (1986) 224.
79. M. YAMASHITA, K. TORIZUKA and T. SATO, *Opt. Letters* **13** (1988) 24.
80. M. YAMASHITA, T. HIRAGA, H. MATSUDA, K. TORIZUKA, S. OKADA, T. MORIYA and H. NAKANISHI, *Opt. Commun.* **79** (1990) 107.
81. S. DE SILVESTRI, P. LAPORTA and O. SVELTO, *Opt. Letters* **9** (1984) 335.
82. V. PETROV, W. RUDOLPH and B. WILHELMI, *J. Mod. Optics* **36** (1989) 587.

83. E. P. TREACY, *IEEE J. Quantum Electron.* **QE-5** (1969) 454.
84. A. LAUBEREAU and D. VON DER LINDE, *Z. Naturforsch.* **25a** (1970) 1626.
85. A. PENZKOFER, *Opt. Quantum Electron.* **23** (1991) to be published.
86. O. SVELTO, *Progress in Optics* **12** (1974) 1.
87. K. B. EISENTHAL, in 'Ultrashort Light Pulses, Picosecond Techniques and Applications', edited by S. L. Shapiro, *Topics in Appl. Phys.*, Vol. 18 (Springer-Verlag, Berlin, 1977) p. 275.
88. R. C. Weast (Ed), 'Handbook of Chemistry and Physics', 1st Student Edition (CRC Press, Inc., Boca Raton, Florida, 1987) p. F-21.
89. B. MEIER and A. PENZKOFER, *Appl. Phys.* **B49** (1989) 513.
90. K. S. BUDIL, I. A. McINTYRE and C. K. RHODES, *Opt. Commun.* **64** (1987) 279.
91. D. L. MACFARLANE, L. W. CASPERSON and S. M. JONES, *IEEE J. Quantum. Electron.* **QE-25** (1989) 2485.
92. N. JAMASBI, J. C. DIELS and L. SARGER, *J. Modern Opt.* **35** (1988) 1891.
93. H. KUBOTA, K. KUROKAWA and M. NAKAZAWA, *Opt. Letters* **13** (1988) 749.
94. W. T. LOTSHAW, D. McMORROW, T. DICKSON and G. A. KENNEY-WALLACE, *Opt. Letters* **14** (1989) 1195.
95. K. KUROKAWA, H. KUBOTA and M. NAKAZAWA, *Opt. Commun.* **73** (1989) 319.
96. F. LAERMER, J. DOBLER and T. ELSAESSER, *Opt. Commun.* **67** (1988) 58.
97. M. MIHAILIDI, Y. BUDANSKY, X. M. ZHAO, Y. TAKIGUCHI and R. R. ALFANO, *Opt. Letters* **13** (1988) 987.
98. P. GEORGES, F. SALIN and A. BRUN, *Opt. Letters* **14** (1989) 940.
99. P. GEORGES, F. SALIN, G. LE SAUX, G. ROGER and A. BRUN, *Opt. Commun.* **69** (1989) 281.
100. P. M. W. FRENCH, A. S. L. GOMES, A. S. GOUVEIA-NETO and J. R. TAYLOR, *Opt. Quantum Electron.* **18** (1986) 171.
101. W. DIETEL, E. DÖPEL, K. HEHL, W. RUDOLPH and E. SCHMIDT, *Opt. Commun.* **50** (1984) 179.
102. P. LAPORTA and V. MAGNI, *Appl. Opt.* **24** (1985) 2014.
103. A. M. WEINER, J. G. FUJIMOTO and E. P. IPPEN, *Opt. Letters* **10** (1985) 71.
104. W. DIETEL, E. DÖPEL, D. KÜHLKE and B. WILHELMI, *Opt. Commun.* **43** (1982) 433.
105. W. DIETEL, J. J. FONTAINE and J. C. DIELS, *Opt. Letters* **8** (1983) 4.
106. J. J. FONTAINE, W. DIETEL and J. C. DIELS, *IEEE J. Quantum Electron.* **QE-19** (1983) 1467.
107. P. M. W. FRENCH, J. A. R. WILLIAMS and J. R. TAYLOR, *Opt. Letters* **12** (1987) 684.
108. P. M. W. FRENCH and J. R. TAYLOR, *Opt. Letters* **13** (1988) 470.
109. G. ANGEL, R. GAGEL and A. LAUBEREAU, *Chem. Phys.* **131** (1989) 129.
110. D. RICARD and J. DUCUING, *J. Chem. Phys.* **62** (1975) 3616.

Appendix A: Rate equations for short-wavelength excitation of DODCI

The short-wavelength excitation scheme of the absorber is shown in Fig. 2a. The corresponding equation system for the absorber bleaching reads

$$\frac{\partial N_{1N}}{\partial t'} = -\frac{\sigma_N}{h\nu_L}(N_{1N} - N_{2N^*})\kappa I_{L,A} + \frac{N_{2N} + N_{2N^*}}{\tau_N} \tag{A1}$$

$$\frac{\partial N_{2N^*}}{\partial t'} = \frac{\sigma_N}{h\nu_L}(N_{1N} - N_{2N^*})\kappa I_{L,A} - \frac{N_{2N^*}}{\tau_{FC}} - \frac{N_{2N^*}}{\tau_N} \tag{A2}$$

$$\frac{\partial N_{2N}}{\partial t'} = \frac{N_{2N^*}}{\tau_{FC}} - \frac{N_{2N}}{\tau_N} \tag{A3}$$

$$\frac{\partial N_{1P}}{\partial t'} = -\frac{\sigma_P}{h\nu_L}(N_{1P} - N_{2P^*})\kappa I_{L,A} + \frac{N_{2P} + N_{2P^*}}{\tau_P} \tag{A4}$$

$$\frac{\partial N_{2P^*}}{\partial t'} = \frac{\sigma_P}{h\nu_L}(N_{1P} - N_{2P^*})\kappa I_{L,A} - \frac{N_{2P^*}}{\tau_{FC}} - \frac{N_{2P^*}}{\tau_P} \tag{A5}$$

$$\frac{\partial N_{2P}}{\partial t'} = \frac{N_{2P^*}}{\tau_{FC}} - \frac{N_{2P}}{\tau_P} \tag{A6}$$

$$\frac{\partial I_{L,A}}{\partial z'} = -I_{L,A}[\sigma_N(N_{1N} - N_{2N^*}) + \sigma_P(N_{1P} - N_{2P^*})] \tag{A7}$$

The parameters and the initial conditions are the same as in the case of long-wavelength excitation.